INTEGRATING INSTRUMENTATION VALIDATION METHODOLOGIES FOR THE RETRIEVAL OF CLOUD TOP PARAMETERS FROM EOS TERRA SENSORS

By

Ana J. Picón Feliciano

A thesis submitted in partial fulfillment of the requirements for the degree of

MASTER OF SCIENCE

In

COMPUTER ENGINEERING

UNIVERSITY OF PUERTO RICO
MAYAGÜEZ CAMPUS
2006

Approved by:

_____	_____
Domingo Rodríguez, Ph.D. Member, Graduate Committee	Date
_____	_____
Jorge E. González, Ph.D. Member, Graduate Committee	Date
_____	_____
Ramón Vásquez, Ph.D. President, Graduate Committee	Date
_____	_____
Vikram Pandya, Ph.D. Representative of Graduate Studies	Date
_____	_____
Isidoro Couvertier, Ph.D. Chairperson of the Department	Date

ABSTRACT

Geostationary and polar-orbiting satellites data can be used to retrieve cloud top properties such as optical thickness, temperature, pressure and height. The Moderate Resolution Imaging Spectroradiometer (MODIS) and the Multi-angle Imaging Spectroradiometer (MISR) are two of the instruments onboard the Terra Earth Observing System (EOS). Algorithms for the retrieval of cloud-top heights have been implemented in order to get a product that can be applied in climate change studies, climate modeling and atmospheric research. The algorithms to retrieve this kind of information are based on CO_2 slicing and stereo matching methods. The objective of this research is to compare MODIS cloud top pressures and MISR cloud top heights over the Caribbean region to evaluate the retrieval performance of both instruments. This research work describes methodologies related with this validation process.

RESUMEN

Los datos de satélites polares y geoestacionarios pueden utilizarse para recuperar propiedades del tope de nubes tales como profundidad óptica, temperatura, presión y altura. El radiómetro MODIS (Moderate Resolution Imaging Spectroradiometer) y el radiómetro MISR (Multi-angle Imaging Spectroradiometer) son dos de los instrumentos a bordo del satélite Terra del sistema EOS (Earth Observing System). Los algoritmos para la recuperación de altura del tope de la nube se han implementado para obtener productos que pueden ser aplicados a estudios de cambio de clima, modelado climático e investigación atmosférica. Los algoritmos que recuperan este tipo de información están basados en métodos de corte en el canal de CO_2 y correspondencia estereoscópica. El objetivo de esta investigación es la comparación de las presiones del tope de nubes de MODIS y las alturas del tope de nubes de MISR en el área del Caribe para evaluar el desempeño de recuperación de ambos instrumentos. Este trabajo de investigación describe las metodologías relacionadas con este proceso de validación.

DEDICATION

To my parents, Ana and Ruben, who have always given me support and have believed in me. To my brother and friend Ruben who has motivated me during this journey.

ACKNOWLEDGEMENTS

I would like to give thanks to Dr. Ramón Vásquez, Dr. Jorge González, Dr. Domingo Rodríguez and Dr. Hamed Parsiani for all their good advice. Special thanks to the Advanced Satellite Products Team and the Cooperative Institute for Meteorological Satellite Studies (CIMSS) at the University of Wisconsin in Madison: Jeffrey Key, Gary Wade, Timothy Schmitt, W. Paul Menzel, Bob Aune, Andrew Heidinger, Wayne Feltz, Jim Nelson and Anthony Schreiner. Thanks to the people involve in this research: Pieter van der Meer and Fran Holt from NOAA NESDIS. Software tools have been provided by the PaSCoR Laboratory at the University of Puerto Rico-Mayagüez. Special appreciations to the EOS Data Gateway administration staff for their technical support during the research time period. This research has been fully supported by the NOAA CREST grant number NA17AE1625.

TABLE OF CONTENT

LIST OF FIGURES

LIST OF SYMBOLS

Roman symbols

a	cloud albedo
A	surface albedo
B	Planck radiance
$\langle C \rangle$	average value within the comparison patch
C_{max}	maximum value within the comparison patch
C_{min}	minimum value within the comparison patch
E	cloud emissivity
f	cloud fraction
g	gravitational acceleration
N	spectral band
P_c	cloud pressure or pressure level
P_s	surface pressure
R	observed radiance or reflectance
R’	air constant
$\langle R \rangle$	average value within the reference patch
R_{bcd}	opaque cloud radiance
R_{clr}	clear sky radiance
R_{max}	maximum value within the reference image
R_{min}	minimum value within the reference image
R_{sim}	simulated reflectance

S	data set
S’	inverse data set
t	fractional transmittance of radiation
T	transmittance of the clouds
$T_{a,s}$	surface temperature
T_b	brightness temperature
$T_{(p)}$	pressure temperature
z	surface altitude
Z	cloud top height

Greek symbols

ε	normal distributed Gaussian measurement noise
λ	wavelength
$\rho_{a,0}$	density of the air
θ	zenith angle
Γ_s	tropospheric lapse rate

Acronyms

ADEOS	Advanced Earth Observing Satellite
AirMISR	Airborne Multi-Angle Imaging Spectroradiometer
AMSR	Advanced Microwave Scanning Radiometer
ASTER	Advanced Spaceborne Thermal Emission and Reflection Radiometer
CIMSS	Cooperative Institute for Meteorological Satellite Studies

ENVI	Environment for Visualizing Images
ERS-2	Earth Remote Sensing satellite
EOS	Earth Observing System
FOV	Field of View
GLCM	Gray-level CO-occurrence Matrix
GOES	Geostationary Observing System
GOME	Global Ozone Measurement Experiment
GPS	Global Positioning System
GSFC	Goddard Space Flight Center
ICESat	Ice, Cloud and Land Elevation Satellite
IDL	Interactive Data Language
IRW	Infrared window
Landsat-7	Land Remote Sensing Satellite
LPDAAC	Land Processes Distributed Active Archive Center
MISR	Multi-Angle Imaging Spectroradiometer
MODIS	Moderate Resolution Imaging Spectroradiometer
NASA	National Aeronautics and Space Administration
NN	Neural Networks
NOAA	National Oceanic and Atmospheric Administration
NSIDC	National Snow and Ice Data Center
NWS	National Weather Service
PaSCoR	Partnership for Spatial and Computational Research
PNN	Probability Neural Network

POLDER	Polarization and Directionality of the Earth's Reflectances
RLRA	Reflecting Level Reference Altitude
ROCINN	Retrieval of Cloud Information using Neural Networks
SOM	Self-Organized feature Map
SVD	Singular Value Decomposition
TOA	Top of Atmosphere
UTC	Coordinated Universal Time
VAS	Visible Infrared Spin-Scan Radiometer Atmospheric Sounder
WT	Wavelet Transform

LIST OF APPENDICES

1 INTRODUCTION

Clouds are aggregates of water droplets or ice crystals that are suspended in the atmosphere. They are formed by condensation or deposition of water vapor in the atmosphere. The study of these atmospheric visible formations is important in the area of meteorology. Clouds absorb and emit infrared radiation in order to enhance the greenhouse effect and increase the Earth's surface temperature. They contribute to the net radiative balance on Earth. Some cloud formation may indicate uplift and expansional cooling of air such as fog. Geostationary and polar-orbiting satellites data can be used to retrieve cloud top properties such as optical thickness, temperature, pressure and height. The Moderate Resolution Imaging Spectroradiometer (MODIS) and the Multi-angle Imaging Spectroradiometer (MISR) are two of the instruments aboard the Terra Earth Observing System (EOS). These sensors can provide cloud top height information globally. In the following sections, the purpose of studying cloud top height retrieval and the significance of the research work are presented.

1.1 Motivation

Climatological observations to identify climate changes over tropical montane cloud forests include cloud height between other related observations. In [Lawton et al, 2001] and [Nair et al, 2000] is presented the climatic impact of tropical lowland deforestation on nearby montane cloud forests. Landsat and the Geostationary Operational Environmental Satellite (GOES) imagery were used to detect the occurrence of cumulus clouds over Nicaragua and Costa Rica. Results show that cumulus clouds formed over

forested regions earlier than over deforested regions. Cloud patterns over this tropical region may indicate that a change in land use can influence the climate at the surrounding montane cloud forests. [González et al, 2005] presents the first case of urban heat island in San Juan, Puerto Rico. The author shows clear evidence of this climate change influenced by the land use over this tropical coastal city. Evidence of a climatic impact over the Luquillo Forest associated to differences in cloud patterns has not been reported. Based on this matter, the motivation of this research is to use cloud top height information over the Caribbean to analyze the climate, to understand the water cycle on rain forests and urban areas and use input information to predict the climate on a tropical island such as Puerto Rico.

1.2 Problem Statement

The algorithms to retrieve cloud top heights from MODIS and MISR are based on CO_2 slicing and stereo matching methods. In MODIS cloud top heights appear in terms of cloud top pressures. MISR cloud top heights are denominated as stereo heights. One main concern about using this climatological information over the Caribbean is to assure the quality of the instruments retrieval. This research work presents the methodologies involved in a validation process to compare the cloud top height retrieval of MODIS and MISR.

1.3 Objectives

The objectives of this research are:

- To implement an algorithm that calculates cloud top heights from MODIS. To compare MISR cloud top heights with MODIS cloud top pressures, an algorithm must be implemented.
- To use the cloud top height estimates to classify different types of clouds in future research work. By evaluating cloud top temperatures and cloud top heights, different types of clouds can be inferred.
- To provide other researchers with a validation mechanism to compare different instruments.
- To validate operational cloud products over mid-latitudes and tropical regions.

1.4 Contribution to the area

By implementing a validation process to assess the retrieval performance of two instruments, two significant improvements overcome from this work. First, due to the lack of a cloud top height dataset in the MODIS cloud product, it is necessary to create a pressure-height converter. The creation of this algorithm will be an extension of the MODIS cloud product. Having retrieved cloud top heights will provide to meteorologists an advantage of this type of parameters from MODIS resulting in a better study of cloud top properties and their effects on the atmosphere. The second improvement overcomes from the development of methodologies required for the instruments validation that will not depend on time limited observations.

1.5 Thesis Overview

Chapter 2 presents a literature review about the different cloud top height techniques and validation efforts. Chapter 3 presents the satellite data resources and software tools that were used in this research. Chapter 4 describes the details of every component in the validation process between the two instruments. Chapter 5 presents the results obtained from the comparison between the two instruments. Chapter 6 presents the conclusions about the research work. Chapter 7 proposes suggestions for future work. Appendices include details about the satellite data management and visualization tools.

2 THEORETICAL BACKGROUND

Cloud top properties can be retrieved by different methods. Data from some satellite sensors such as MODIS, Geostationary Observing System 12 imager (GOES-12 imager) and the Visible Infrared Spin-Scan Radiometer Atmospheric Sounder (VAS) is used to assign cloud heights and velocities of cloud motion vectors based on calculations from the radiative transfer equation. Some methods such as the window channel estimate, the CO_2 slicing and H_2O-IRW intercept are applied to calculate cloud top pressures. The reflected light polarization is another technique used to detect cloud top phase information from the Polarization and Directionality of the Earth's Reflectances (POLDER) sensor onboard the Advanced Earth Observing Satellite (ADEOS). In some other cases in which the sensors don't have the capability of water vapor or infrared channels, geometric methods are used such as stereophotogrammetric measurements. Neural networks methods have also been used to retrieve cloud top parameters. The following sections present different cloud top height retrieval techniques.

2.1 Window Channel Estimate

In [Nieman et al., 1993] is presented an estimate that compares infrared window (11.2 μm) brightness temperatures with numerical model forecast temperature profiles to infer the level of best agreement. The brightness temperature T_b in the infrared window is an overestimate of the cloud temperature. Heights are then inferred from T_b and an available temperature profile. The temperature profile used in this work was a 6 hours forecast model.

2.2 H_2O-IRW Intercept Method

In [Nieman et al., 1993] is presented an interception based method. Radiances in one spectral band observing a single cloud layer will vary linearly with the radiances in another spectral band as a function of cloud amount in the FOV. By plotting radiances from the H_2O channel at 6.7 μm vs. radiances from the IRW channel at 11.2 μm, a nearly linear relationship can be obtained. Radiance measurements will be used for the radiative transfer calculations for both spectral channels. The intersection of measured and calculated radiances will occur at clear-sky and opaque cloud radiances. Clear sky radiances will have a cloud amount of zero and opaque cloud radiances a cloud amount of one. The cloud-top temperature will be extracted from this intersection. Figure 2.1 is presented in [Nieman et al, 1993] and shows an example of intersection between the two channels. A line intersects the curve of calculated radiances when radiances emanate from the surface (clear sky) and from an opaque cloud at the correct pressure. Measured radiances used to relate both spectral bands radiances are the average radiances for the cluster of clearest (warmest) field of view and the cluster of the cloudiest (coldest) field of view in the observed area. When the calculated H_2O radiances for clear sky are less than the measured H_2O radiances, calculated H_2O radiances are adjusted to agree with the measured clear-sky H_2O radiances. The difference can be caused by an inaccurate guess profile that is used in the calculation of clear sky radiance. Figure 2.2 is also presented in [Nieman et al, 1993] and shows the calculated radiances curve and the adjusted radiances curve. Calculated warm radiances that are greater than measured radiances are not adjusted if the low measurement may result from cloud contamination.

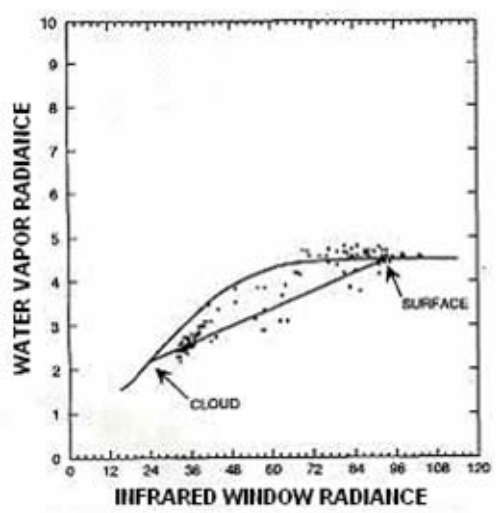

Figure 2.1 Measured radiances (mW cm/m^2 sr) for FOVs partially filled with clouds presented in [Nieman et al., 1993].

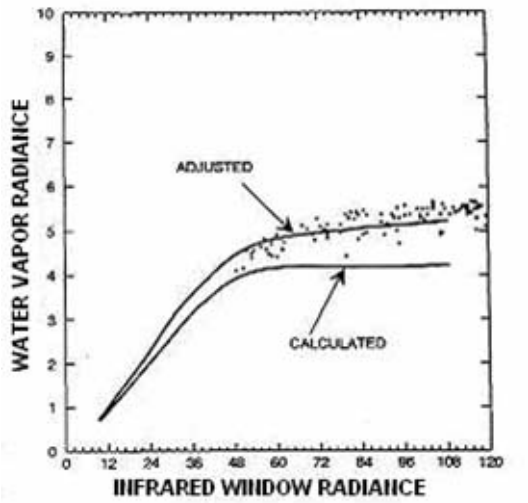

Figure 2.2 Adjustment of H2O radiance (mW cm/m2 sr) when calculated and measured values disagree presented in [Nieman et al., 1993].

2.3 Reflected Light Polarization

Cloud detection and distinction of water/ice-phase of cloud top can be determined by using polarized reflectance at 0.865μm of the Polarization and Directionality of the

Earth's Reflectances (POLDER) sensor and brightness temperature at 10.9 μm of the OCTS sensor, both onboard the Advanced Earth Observing Satellite (ADEOS). In [Yasumoto et al., 2001] is presented this cloud top phase retrieval technique. The algorithm for cloud detection is based on a sequential test using each threshold value for each item from the POLDER and OCTS cloud coverage maps. In the case of the POLDER sensor, the cloud coverage map is derived from the reflectance and polarized reflectance at 0.865μm. In the case of OCTS sensor, the cloud coverage map is derived from the brightness temperature at 10.9 μm. After the cloud detection process, each cloud pixel is examined to determine the thermodynamic phase of the cloud top by using both sensors cloud data. Single scattering simulations of polarized reflectance are compared with the polarized reflectance at 0.865μm to distinguish water and ice clouds. Differences between the angular tendency of polarized reflectance from water clouds and the angular tendency of polarized reflectance from ice clouds are used to distinguish the cloud thermodynamic phase by looking at the observed data and the simulated values.

2.4 Stereo Matching Method

MISR has nine cameras Df, Cf, Bf, Af, An, Aa, Ba, Ca and Da (from the most forward to the most aftward looking). Each camera is positioned to a different angle. A combination of nine cameras and 4 spectral bands will result in 36 different channels. Cloud information can be retrieve from the 0.67μm spectral band. The conceptual methodology of the cloud-top height retrieval using MISR data is described in [Moroney et al., 2002] and [Muller et al., 2002]. It is mentioned that the image data is broken into

144 blocks of equal area. Each block is 140.8 km long and 563.2 km wide and covers the same geographical location for all the nine cameras. It is also mentioned that each block will be subdivided into 16 mesoscale domains (70.4 km on a side) and wind vectors will be retrieved in an independent form for every domain. After determining the cloud advection field, a stereo-matching algorithm is used in Bf-Df and Bf-An camera pairs. Matched points will be used to solve cloud-motion and cloud-top height. The camera pairs Af-An and Aa-An are used independently in the stereo matcher. The height field will be retrieved for each fourth pixel. Figure 2.3 shows the implementation of the MISR cloud-top height retrieval algorithm. The mathematical formulations for this methodology are described in [Zong et al., 2002].

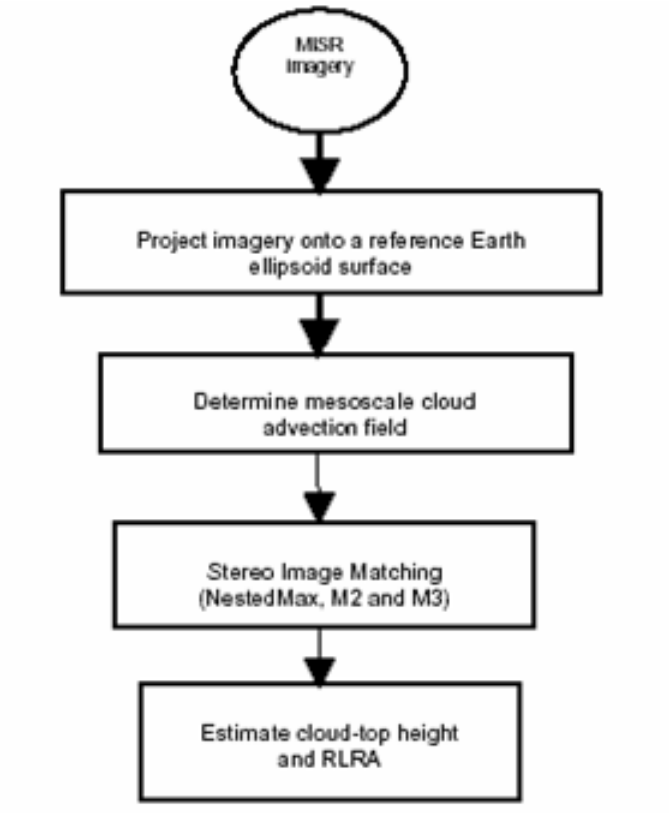

Figure 2.3 Schematics of MISR cloud-top height retrieval algorithm.

One of the stereo algorithms is NestedMax. It is a feature-matcher used to retrieve wind vectors. The area matchers are M2 and M3. They are used to retrieve cloud height. The metrics for M2 and M3 are computed for each pair, and then the one with the lowest metric value is chosen as the best match. Metric values of 0.75 and 1.0 are used for M2 and M3. The M2 and M3 metrics are defined in [Muller et al., 2002] as follows:

$$S_{M2} = \frac{\sum_{i,j}\left|\left[\frac{R(x_i,y_i)-\langle R\rangle}{R_{max}-R_{min}}\right]-\left[\frac{C(x_i,y_i)-\langle C\rangle}{C_{max}-C_{min}}\right]\right|}{\sigma_{M2}} \quad 2.1$$

$$\sigma_{M2} = \sum_{i,j}\left|\left[\frac{R(x_i,y_i)-\langle R\rangle}{R_{max}-R_{min}}\right]\right| \quad 2.2$$

$$S_{M3} = \frac{\text{median}_{ij}\left\{\left|\frac{R(x_i,y_i)}{\text{median}(R)}-\frac{C(x_i,y_i)}{\text{median}(C)}\right|\right\}}{\sigma_{M3}} \quad 2.3$$

$$\sigma_{M3} = \text{median}_{ij}\left\{\left|\frac{R(x_i,y_i)}{\text{median}(R)}-1\right|\right\} \quad 2.4$$

$R(x_i,y_i)$ are the reference pixel values at (i,j), $C(x_i,y_i)$ are the corresponding values in the comparison image, R_{max} and R_{min} are the maximum and minimum values within the reference image, C_{max} and C_{min} are the maximum and minimum values within the comparison patch, $\langle R\rangle$ is the average value within the reference patch, $\langle C\rangle$ is the average value within the comparison patch and i,j are relative indices within the patches for summation. For every pixel with a valid stereo retrieval, the height is calculated by suing the wind value that was previously determined for the pixel to correct the retrieved

disparities for the cloud motion. When one camera pair has a valid retrieval, the height is accepted. When both camera pairs from the forward and aftward angles have valid heights, the difference between in both heights is compared against a pixel dependent threshold. If both heights agree, the higher will be the Reflecting Layer Reference Altitude (RLRA). If they don't agree, they're rejected. In Figure 2.4, stereo heights (right image) are calculated over the region indicated in the map (left image) that corresponds to path 3 during February 12, 2004 at 14:25:40 GMT, blocks 62-80.

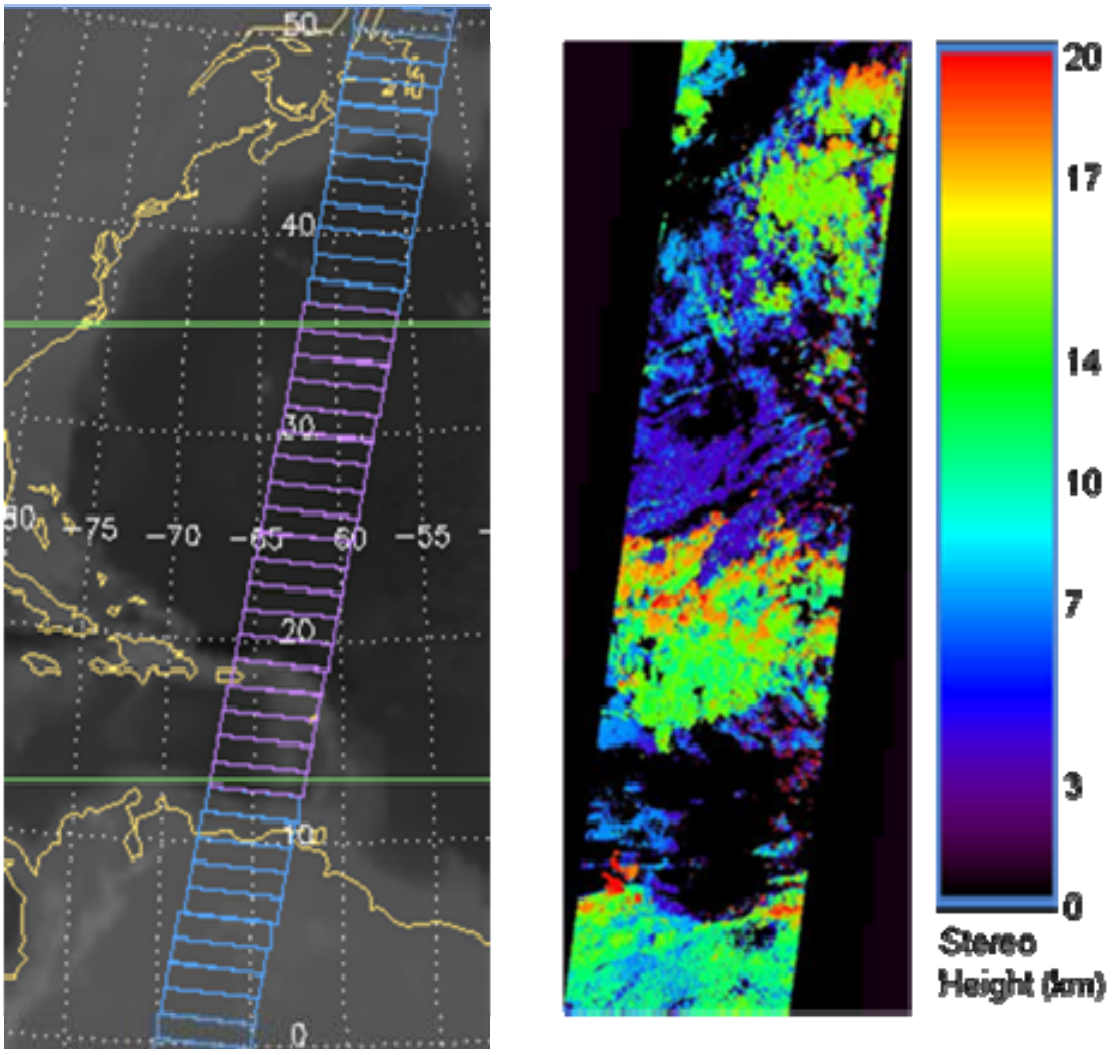

Figure 2.4 Stereo heights measured from the MISR sensor. Region covered by the image (left side). Calculated stereo heights (right side).

2.5 Cloud Classification Based on Neural Networks

A cloud classification system is presented in [Tian et al., 1997]. Two image transformation schemes Wavelet Transform (WT) and Singular Value Decomposition (SVD) are used to extract the textural feature of the data and are compared with those of the well-known Gray-level CO-occurrence Matrix (GLCM) approach. Two different neural networks: the probability neural network (PNN) and the unsupervised Kohonen self-organized feature map (SOM) are used and examined. The performance of the proposed cloud classification system is benchmarked on the Geostationary Operational Environmental Satellite (GOES) 8 data set showing good results. Different from the other presented methods, instead of using a spectral feature analyzer, the author proposed the use of a textural feature analyzer. With textural features, it can be distinguished certain types of clouds by the spatial distribution characteristics of gray levels corresponding to a single region within the image. The Gray-level CO-occurrence Matrix approach uses statistical measures to characterize textural features. The Wavelet Transform is a texture analysis scheme that reduces the dimensionality of the data. The Single Value Decomposition is an excellent tool for image restoration and data reduction. The Kohonen self-organized feature map is an unsupervised neural network. The Probability Neural Network is a supervised network.

In [Loyola, 2004] is presented an algorithm based on neural networks techniques to determine the cloud top height and the cloud top albedo by using spectral information in the Oxygen A-band in and around 760nm. The algorithm is called ROCINN which means Retrieval of Cloud Information using Neural Networks. It solves the inverse

problem using neural networks which was first presented in [Loyola, 2001]. Beginning with the Earth's reflectance R at the top of the atmosphere that is defined as

$$R(\lambda) = \frac{I(\lambda)}{I_0(\lambda)\cos(\theta_0)\pi} \quad 2.5$$

The average transmittance through the band can define a relationship between cloud fraction, cloud top height and cloud top albedo. Then, the simulated reflectance R_{sim} can be defined as

$$R_{sim} = (1-f)T(\lambda,\theta_0,\theta,A,Z) + fT(\lambda,\theta_0,\theta,a,z) \quad 2.6$$

where f is the cloud fraction, T is the transmittance of the clouds, λ is the wavelength, θ_0 is the solar zenith angle, θ is the satellite zenith angle, A and a are the surface and cloud top albedos respectively, Z is the surface altitude, and z is the cloud top height. The algorithm takes the cloud fraction as input and computes the cloud top height and the cloud top albedo. The radiative transfer model function computing reflectance can be represented by the data set S which is defined as

$$S = \{(X_i, Y_i)\} \text{ for i =1,…,t} \quad 2.7$$

The input X are the parameters $f, \theta_0, \theta, \phi, A, Z, a$ and z. The output Y are the simulated radiances $R_{sim}(\lambda)$. An inverse data set is generated by adding to the simulated reflectance a normal distributed Gaussian measurement noise ε.

$$R = R_{sim} + \varepsilon \quad 2.8$$

The inverse data set generated is defined as

$$S' = \{(X_i', Y_i')\} \text{ for i =1,…,t} \quad 2.9$$

The input X' are the parameters R (λ), $f, \theta_0, \theta, \phi, A$ and Z. The output Y' are the cloud top albedo a and the cloud top height z. Finally a neural network (NN) is trained with the inverse data set S'. The cloud top height and the cloud top albedo will be computed as follow

$$(a, z) = NN\left(R(\lambda), f, \theta_0, \theta, \phi, A, Z\right) \qquad 2.10$$

Results from the ROCINN algorithm are shown in Figure 2.5. Cloud top heights were calculated by using imagery from the Global Ozone Measurement Experiment (GOME) onboard the Earth Remote Sensing satellite (ERS-2). The ROCINN algorithm was compared with cloud information obtained by the FRESCO algorithm and with a cloud product from the ATSR-2 instrument onboard also in the ERS-2. Results were observed during July 15, 1998. ROCINN algorithm shows more stability than the FRESCO algorithm. ATSR-2 and ROCINN shows similar results.

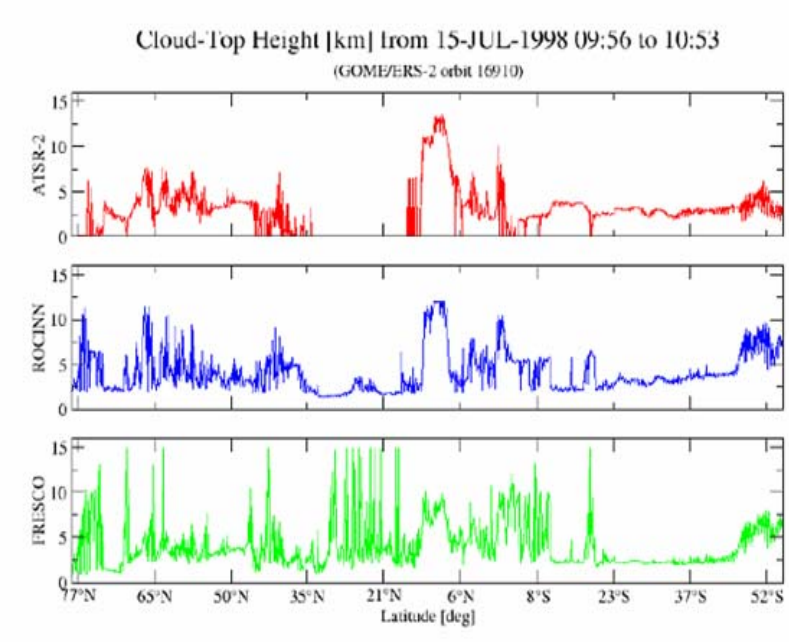

Figure 2.5 Comparison of the three techniques presented in [Loyola, 2004] for the GOME cloud top height retrieval.

3 MATERIALS AND EQUIPMENT

The satellite data recollection and management and the implementation of the algorithms were tasks performed in two of the laboratories in the University of Puerto Rico at the Mayagüez Campus (UPRM): the Climatology Laboratory and the PaSCoR (Partnership for Spatial and Computational Research) Laboratory. The Climatology Laboratory is located at the Department of Mechanical Engineering Building. The main server called Climatemaster is SUN Solaris SO UNIX with 6 terminals. The system includes C/C++ and FORTRAN compilers and MATLAB. Two other terminals are Windows XP operated and are connected to the Mechanical Engineering network server. The PaSCoR Laboratory is located at the Department of Electrical and Computer Engineering Building. The system is Windows XP operated. Most of the available software is for the georegistration, processing and visualization of multiple data sources such as radars, antennas, satellites, aircrafts, etc. The software includes ERDAS, ArcView/ArcMap, Idrisi and ENVI. Some of the available data sources include aerial photograph of the Puerto Rico area, IKONOS images, orographic maps and GPS (Global Positioning System) georeferenciation systems. The algorithms presented in this work were implemented with the help of MATLAB and ENVI. Satellite data was ordered through an ftp site of the EOS Data Gateway. Upper Air observations were recollected from the University of Wyoming Weather Site.

3.1 Earth Observing System

The Earth Observing System (EOS) is a NASA program created in 1958. NASA scientists has been studying the Earth and its changing environment by observing the atmosphere, oceans, land, ice, and snow, and their influence on climate and weather. The key to better understand the global environment is by exploring how the Earth's systems such as air, land, water, and life interact with each other. This approach is called the Earth System Science and blends together fields like meteorology, oceanography, biology, and atmospheric science.

In 1991, NASA announced a comprehensive program to study the Earth as an environmental system and was called the Earth Science Enterprise. By using satellites and other tools to study the Earth, the scientists can have a better understanding of how natural processes affect humans, and how humans might be affecting them. Such studies will yield improved weather forecasts, tools for managing agriculture and forests, information for fishermen and local planners, and, eventually, the ability to predict how the climate will change in the future.

The Earth Science Enterprise has three main components: a series of Earth-observing satellites, an advanced data system, and teams of scientists who will study the data. Key areas of study include clouds; water and energy cycles; oceans; chemistry of the atmosphere; land surface; water and ecosystem processes; glaciers and polar ice sheets; and the solid Earth. The phase 1 of the Earth Science Enterprise was comprised of focused, free-flying satellites, space shuttle missions, and various airborne and ground-based studies. The phase 2 began in December 1999 with the launch of the first Earth

Observing System (EOS) satellite Terra (formerly AM-1). EOS is the first observing system to offer integrated measurements of the Earth's processes. It consists of a science component and a data system supporting a coordinated series of polar-orbiting and low-inclination satellites for long-term global observations of the land surface, biosphere, solid Earth, atmosphere, and oceans. An era of unprecedented observational capability for understanding the planet has been initiated. The elements of the Earth Science Enterprise will expand the perspective of the global environment and climate.

3.2 MODIS

The Moderate Resolution Imaging Spectroradiometer is one of the EOS facility instruments that was designed to measure biological and physical processes on a global basis every one to two days. The instrument was developed to be onboard Terra and Aqua satellites. It provides long-term observations used to understand the global dynamics and processes occurring on the surface of the Earth and in the lower atmosphere. It is a multidisciplinary observer of high-priority atmospheric, oceanic, and land-surface features such as cloud cover in the case of atmosphere, sea-surface temperature in the case of the ocean and land cover changes in the case of the land.

It employs a conventional imaging-radiometer concept that consists of a cross-track scan mirror and collects optics, and a set of linear detector arrays with spectral interference filters located in four focal planes. The optical arrangement provides imagery in 36 discrete bands from 0.4 to 14.5 micrometers. Its physical size is 1.044 x 1.184 x 1.638 meters. Its total mass is 229 kilograms. The spectral bands have spatial resolutions

of 250 meters, 500 meters, and 1 kilometer at nadir (90° angle), signal-to-noise ratios of greater than 500 at 1 kilometer resolution(at a solar zenith of 70°); and absolute irradiance accuracies of ±5 percent from 0.4 to 3 micrometers and 1 percent in the thermal infrared(3 to 14.5 micrometers).

Some of the MODIS products are made over weekly to monthly time intervals. These products are used for seasonal phenomena studies. The purpose of these products is to reduce data volume and provide cloud-free coverage over a defined time period. MODIS provides specific global data products including surface temperature with 1 kilometer resolution for day and night; ocean color; chlorophyll fluorescence within 50 percent at surface-water concentrations of 0.5 mg m^{-3}; concentrations of chlorophyll a within 35 percent, vegetation/land-surface cover, conditions and productivity; snow cover and sea ice cover; land-surface reflectance with bidirectional reflectance and albedo; cloud cover with 250 meters resolution by day and 1,000 meters resolution by night; cloud properties characterized by cloud-droplet phase, optical thickness, droplet size, cloud-top pressure, and emissivity; aerosol properties defined as optical thickness, particle size, and mass transport; fire occurrence, size, and temperature; global distribution of precipitable water; and cirrus-cloud cover.

3.3 MISR

The Multi-angle Imaging Spectroradiometer (MISR) is another of the facility instruments onboard EOS TERRA. Routinely it provides multiple-angle, continuous sunlight coverage of the Earth with high spatial resolution. It obtains multidirectional observations of each scene within a time scale of minutes under the same atmospheric

conditions. Its physical size is 0.9 meters wide by 0.9 meters high by 1.3 meters long. Its total mass is 149 kilograms. The instrument has nine individual charge-coupled device(CCD)-based pushbroom cameras to observe the Earth at nine discrete view angles: one at nadir, and eight at other symmetrical views at 26.1°, 45.6°, 60.0°, and 70.5° forward and aftward of nadir. The images at each angle will be obtained in four spectral bands centered at 446, 558, 672, and 866 nanometers. Each of the 36 instrument data channels (4 spectral bands x 9 cameras) individually provides ground sampling of 275 meters, 550 meters, or 1.1 kilometer. The swath width of the imaging data is 360 kilometers and provides global multi-angle coverage of the entire Earth in 9 days at the equator, and 2 days at the poles.

Instrument design and calibration strategies have the goal to maintain absolute radiometric uncertainty to less than ±3% over bright surfaces and ±6% over dark surfaces, with smaller uncertainties in relative band-to-band and angle-to-angle radiances. MISR images are acquired in two observing modes: global and local. Global Mode provides continuous planet-wide observations. Local Mode provides data at the highest resolution in all spectral bands and all cameras for selected 300 kilometers x 300 kilometers regions. Global Mode data is used to generate two standard Level 2 science products during ground data processing: the Top-of-Atmosphere (TOA)/Cloud Product and the Aerosol/Surface Product.

The objective of the TOA/Cloud Product is to enable study, on a global basis, of the effects of different types of cloud fields(classified by their heterogeneity and altitude) on the solar radiance and irradiance reflected to space, and to determine their effects on the Earth's climate. It also provides a cloud screen for MISR aerosol and surface retrievals.

The aerosol parameters of the Aerosol/Surface Product enable the study on a global basis of the magnitude and natural variability in space and time of sunlight absorption and scattering by aerosols in the Earth's atmosphere, especially in the troposphere, and to determine their effects on climate. Surface parameters of the Aerosol/Surface Product enable improved measures of land-surface characteristics, particularly bidirectional and hemispherical reflectances, leaf area index, surface-cover type, and fractional absorbed photosynthetically active radiation, on a global basis; to provide, in combination with MODIS, improved measures of land-surface classification, dynamics, and over vegetated terrain, canopy photosynthesis and transpiration rates; and to supplement MODIS studies of the biogeochemical cycle in the tropics by providing atmospherically corrected ocean color data.

3.4 EOS Data Gateway

The EOS Data Gateway can be accessed via Internet through the address http://edcimswww.dr.usgs.gov. The user can search for and order earth science data products from NASA and affiliated centers. Some of the affiliated centers are Goddard Space Flight Center (GSFC), Land Processes Distributed Active Archive Center (LPDAAC) and the NSIDC. This data gateway provides the interaction of the user with the different NASA centers to download specific data products from different satellite sensors such as MODIS, MISR, AMSR, ASTER, Landsat-7 and ICESat (Ice, Cloud, and Land Elevation Satellite).

3.5 Radiosonde Observations

During 60 years, the National Weather Service (NWS) has been observed the upper air level by the use of radiosonde equipment. The radiosonde is a small instrument package that is suspended below a 2 meter (6 feet) wide balloon filled with hydrogen or helium. As the radiosonde is carried all the way up, sensors inside the instrument package measure profiles of pressure, temperature, and relative humidity. These sensors are linked to a battery powered, 300 milliwatt radio transmitter that sends the sensor measurements to a sensitive ground receiver on a radio frequency ranging from 1668.4 - 1700.0 MHz(see figure 3.1). Information on wind speed and direction aloft is obtained by tracking the position of the radiosonde in flight. Observations where winds aloft are also obtained are called "rawinsonde" observations.

The radiosonde flight can last about two hours, and during this time the radiosonde can ascend to over 35 km (about 115,000 feet) and drift more than 200 km (about 125 miles) from the release point. During the flight, the radiosonde is exposed to temperatures as cold as -90 ^{o}C (-130 ^{o}F) and an air pressure as low as 20 milibar (20 hPa). When the balloon has expanded beyond its elastic limit and bursts (about 6 m or 20 feet in diameter), a small parachute slows the descent of the radiosonde, minimizing the danger to lives and property.

Although all the data from the flight are used, data from the surface to the 400 hPa pressure level (about 7 km or 23,000 feet) are considered minimally acceptable for NWS operations. A flight may be deemed a failure and a second radiosonde is released if the

balloon bursts before reaching the 400 hPa pressure level or if more than 6 minutes of pressure and/or temperature data between the surface and 400 hPa are missing. Worldwide, there are about 900 upper-air observation stations. Most are located in the Northern Hemisphere and all observations are usually taken at the same time each day (00:00 and/or 12:00 UTC), 365 days a year. Observations are made by the NWS at 92 stations - 69 in the conterminous United States, 13 in Alaska, 9 in the Pacific, and 1 in Puerto Rico. NWS supports the operation of 10 other stations in the Caribbean. Radiosonde observations are applied to a broad spectrum of efforts. Data applications include: input for computer-based weather prediction models; local severe storm, aviation, and marine forecasts; weather and climate change research; input for air pollution models; and ground truth for satellite data. Information from related pressure levels and height levels can be inferred from radiosonde observations.

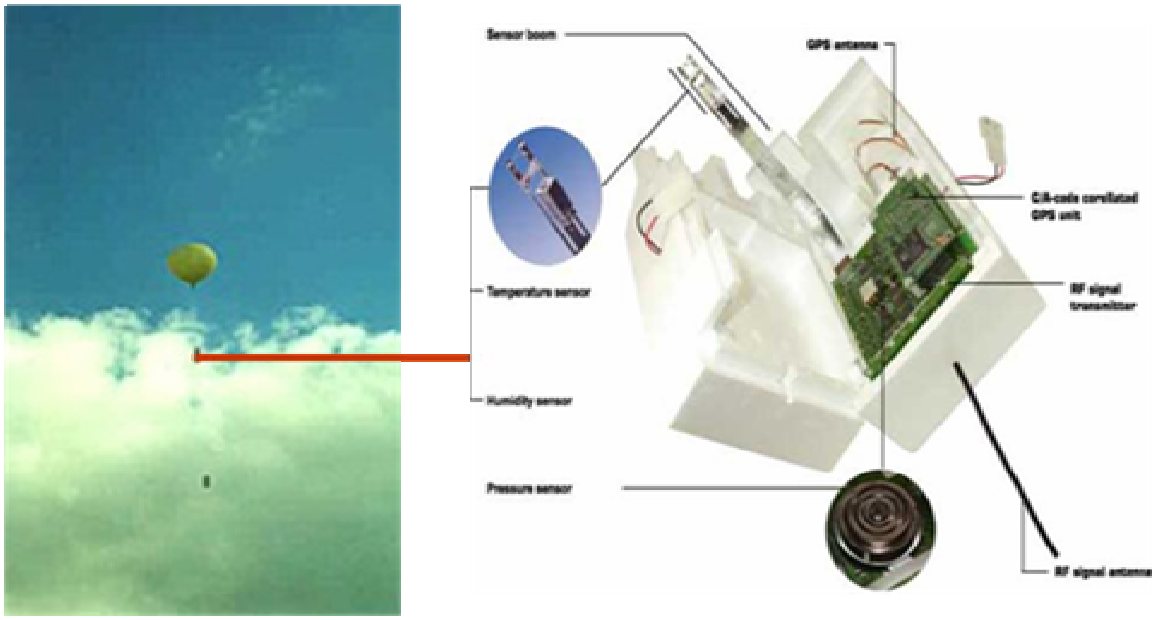

Figure 3.1 Radiosonde instrument.

4 METHODOLOGY

There are several differences between the MODIS and MISR techniques. In the implementation of the algorithm with MISR data, stereo matching methods are employed (see section 2.3). For the case of MODIS, the calculation of radiances is used (see section 4.1). The estimation of cloud heights in MISR is in terms of meters. In MODIS, the estimation of cloud pressures is in terms of Pa. Figure 4.1 shows the implementation for the comparison of these two techniques. Cloud top pressure estimates are based on the CO_2 slicing method. They're available from the MODIS Cloud Product. MODIS and MISR cloud products were ordered through the EOS Data Gateway (for more information see section 3.4). Cloud top height was estimated by implementing an algorithm that is presented in section 4.2. The process of georectification and extraction is presented in section 4.3. Discussion of the analysis process is presented in section 4.4.

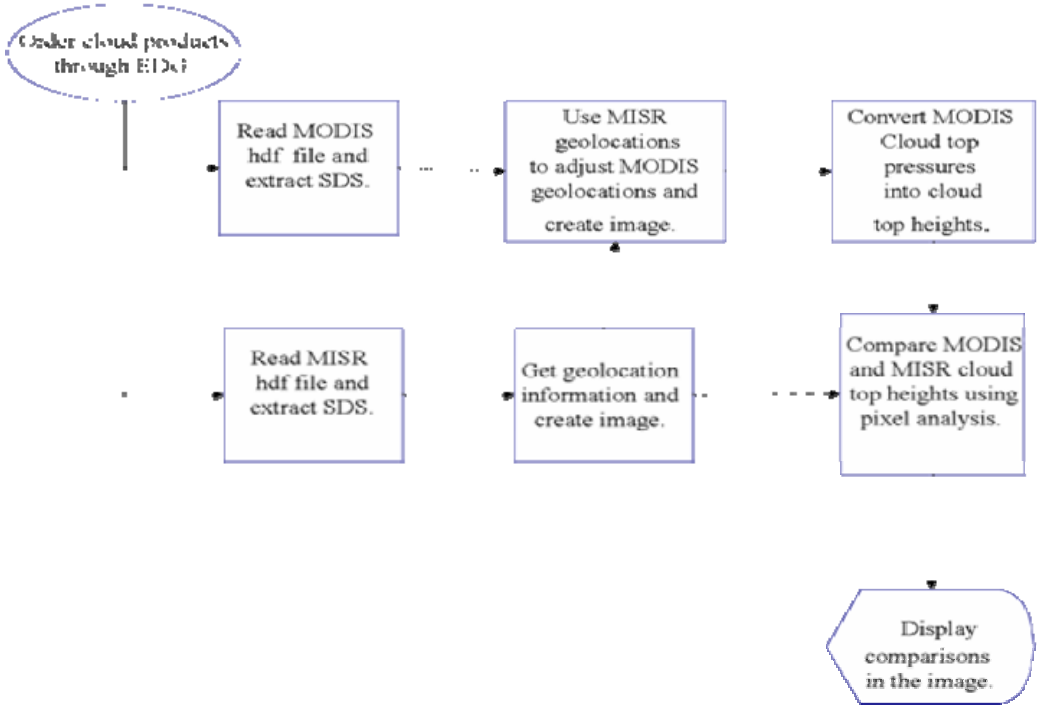

Figure 4.1 Implementation of the cross-comparison between the techniques.

4.1 Cloud Top Pressure Estimation

In [Baum et al., 2002], [Menzel et al., 1997] and [Platnick et al., 2003,] this technique is presented. It calculates the spectral radiative transfer in an atmosphere with a single high cloud layer. For a given cloud element in a field of view (FOV) the radiance observed R(N) in spectral band N is expressed as:

$$R(N) = (1 - nE)R_{cl}(N) + nER_{bcd}(N, P_c) \qquad 4.1$$

where $R_{cl}(N)$ correspond to the clear sky radiance, $R_{bcd}(N,Pc)$ correspond to the radiance where the FOV is completely covered by an opaque or black cloud at pressure level P_c, n is the fraction of the FOV covered with cloud and E is the cloud emissivity. Opaque cloud radiance can be calculated from

$$R_{bcd}(N, P_c) = R_{cl}(N) - \int_{P_c}^{P_s} t(N, p) \frac{dB\left[N, T(p)\right]}{dp} dp \qquad 4.2$$

where P_s is the surface pressure, P_c is the cloud pressure, t(N,p) is the fractional transmittance of radiation of spectral band N emitted from the atmospheric pressure level p arriving at the top of the atmosphere (p=0), and B[N,T(p)] is the Planck radiance of spectral band N for temperature T(p). To determine the cloud-top pressure, first the difference between clear and cloudy radiances is measured from the infrared window at 11.2 μm and the CO_2 channel at 13.3 μm. By equating the measured and calculated ratios of IRW and CO_2 channel radiances differences, the following expression results:

$$\frac{R(CO_2) - R_{cl}(CO_2)}{R(IRW) - R_{cl}(IRW)} = \frac{nE(CO_2)\left[R_{bcd}(CO_2, P_c) - R_{cl}(CO_2)\right]}{nE(IRW)\left[R_{bcd}(IRW, P_c) - R_{cl}(IRW)\right]} \qquad 4.3$$

Because emissivities of clouds and the cloud fraction for the two channels are basically the same, the cloud-top pressure of the cloud can be specified. The left side of the equation is evaluated using measured radiances and clear radiances for the two channels. These are inferred from a sounding and analyzed surface temperatures interpolated to the target point. The right side is computed for a series of possible cloud pressures. The cloud tracer is assigned the pressure that best satisfies the equation. The 13.3 μm channel is sensitive to radiation emitted from most tropospheric features, thus the transmittance through the atmosphere is different enough from the 11 μm channel to produce a significant contrast. In the case of retrieving cloud top pressures from MODIS, they are calculated for the following band pairs: 14.2μm/13.9μm, 13.9μm/13.6μm, 13.6μm/13.3μm, 13.9μm/13.3μm, and 13.3μm/11μm. Emission and absorption of the cloud are assumed to be identical for all band pairs.

4.2 Cloud Top Height Estimation

Three different estimates were done to measure cloud top heights from MODIS by having cloud top pressures. The first estimate was done by deriving the hydrostatic balance equation which is defined as

$$\frac{\partial p}{\partial z} = -\frac{\rho}{R'T} g \qquad 4.4$$

where $T = T_{a,s} - \Gamma_s z$ 4.5

and Γ_s is the tropospheric lapse rate (6.5K km^{-1}).

The equation can be expressed as 4.6 by taking the natural logarithm and then expressed as 4.7 by solving z.

$$In\left(\frac{p_d}{p_{d,s}}\right)=\frac{g}{\Gamma_s R'}In\left(\frac{T_{a,s}-\Gamma_s z}{T_{a,s}}\right) \quad 4.6$$

$$z=\frac{T_{a,s}}{\Gamma_s}\left[1-\left(\frac{p_d}{p_{d,s}}\right)^a\right] \quad 4.7$$

where $a=\frac{\Gamma_s R'}{g}$ 4.8

The second calculation derives the hydrostatic balance equation by interpolation. The hydrostatic balance equation is also defined as 4.9.

$$\frac{\partial p}{\partial z}=-\rho g \quad 4.9$$

By deriving 4.9 in terms of interpolation, it gives 4.10

$$\frac{\partial p_a}{\partial z}\approx\frac{p_{a,1}-p_{a,0}}{z_1-z_0}=-\rho_{a,0}g \quad 4.10$$

where z_1 and z_0 are the desired cloud height and the surface elevation, $\rho_{a,0}$ is the density, $p_{a,1}$ is the desired pressure, $p_{a,0}$ is the surface pressure, g is the gravitational acceleration and $\frac{\partial p_a}{\partial z}$ is the pressure at a given altitude.

The radiosonde (third) estimate was made as follows. During a radiosonde experiment, observations from pressure levels such as 1000, 925, 850, 700, 500, 400, 300, 250, 200, 150, 100, 70, 50 and 10 milibars are mandatory. From these pressure levels, observations about height are defined. Cloud top pressure from MODIS is located between every two consecutive mandatory pressure levels. MODIS pressure is subtracted from the lowest mandatory pressure level and then the difference is multiplied by 45 (between two mandatory pressure levels every milibar equals 45 feet). The related height

to the highest mandatory pressure level is subtracted from the new value. The result is the desired cloud top height in feet units. To get the cloud top height in meter units, the result is multiplied by 3.3.

4.3 Georeferencing Different Data Sources

MISR sensor is looking at the same location on Earth every 16 days; it will be looking the Caribbean at different paths. Image 4.2 shows the paths for the fifth day. MODIS sensor is looking at the Caribbean up to twice a day at different swaths. Because MISR and MODIS sensors are onboard the EOS Terra, MODIS cloud data can be selected at the same dates and similar hours that matched MISR cloud data.

To project MODIS cloud top pressures into a MISR path size, ENVI software can be used to create a new image. Upper left and lower right geographic coordinates from the MISR path must be known to define the new boundaries of MODIS cloud top pressure image. ENVI has a utility to save the data in different file formats. Because MODIS cloud top pressures will be read in Matlab, the file format that will not loss geographic coordinates and pressure values from the extracted data is the geotiff format. Appendix B describes in detail how the data was managed in ENVI and Matlab software.

MISR cloud data file contain 144 blocks that covered high and low latitudes. Because the observed region is the Caribbean, one of the software in IDL, MISR_VIEW is used to extract tropical MISR blocks that will be correlated with MODIS cloud data. Taking selected blocks from MISR data will simplify the data dimensionality to two. A two-dimensional image can be seen in Matlab as a matrix. More information about the management of MISR data is presented in Appendix A.

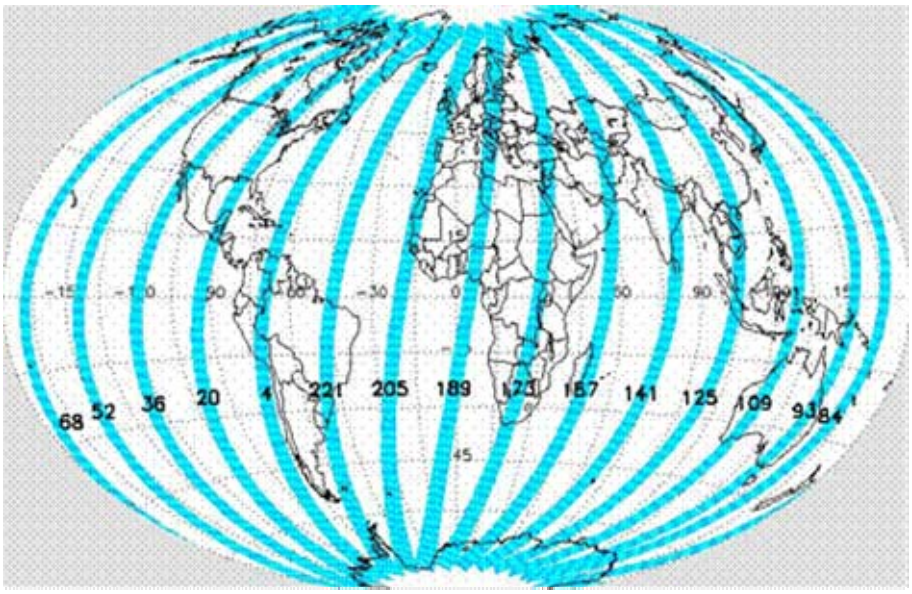

Figure 4.2 Paths from MISR Day Five presented in [Picón, 2004]

4.4 Comparing Different Data Sources

Because the availability of Caribbean cloud top height vertical/horizontal profiles is poor, a cross-comparison between the two radiometers will seek the validation of them. The first step is the calculation of every MODIS pixel with its corresponded MISR pixel. With the error information, two situations can be identified: when both sensors retrieve the same cloud type and when both sensors retrieve different cloud types. By classifying the cloud top level extents in three different ranges, more different situations can be identified. For example, from a range of 3000 meters to 9000 meters, MISR cloud heights were lower than MODIS cloud heights in 10.34% of the cases. This type of analysis will lead to get more accurate results for seeking the validation of the radiometers.

5 RESULTS

Cloud top pressures from MODIS were converted into heights by using three different calculations as described in the methodology section. The time period that was observed correspond to February 12, 2004 to February 16, 2004. During this period, several radiosonde observations were taken at the National Weather Service (NWS) San Juan Airport Station (78526). Figure 5.1 shows the cloud top pressure observed at the San Juan Airport Station by MODIS and figure 5.2 shows the estimated cloud top height by the radiosonde observation, the estimated cloud top height by the Hydrostatic Balance Equation with interpolation (HBEinterpolation), the estimated cloud top height by the Hydrostatic Balance Equation with the free-tropospheric lapse rate (HBElapserate) and an adjustment to the free-tropospheric lapse rate (HBEadjustedlapserate). The cloud top heights estimated by the Hydrostatic Balance Equation with the free-tropospheric lapse rate show better agreement with the estimated cloud top heights with the radiosonde observations.

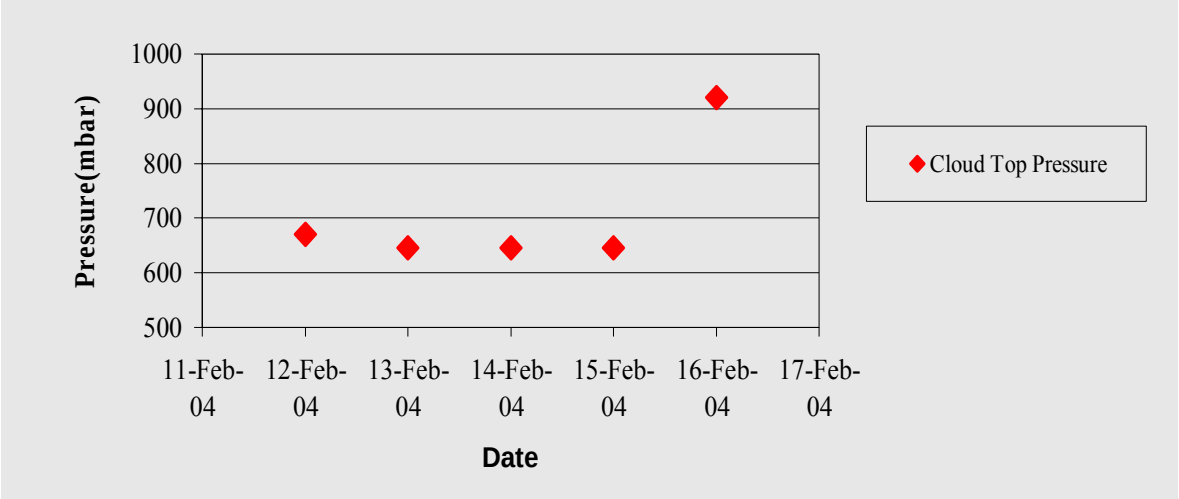

Figure 5.1 Cloud top pressure measured at the same geographic coordinates of the San Juan Airport Station.

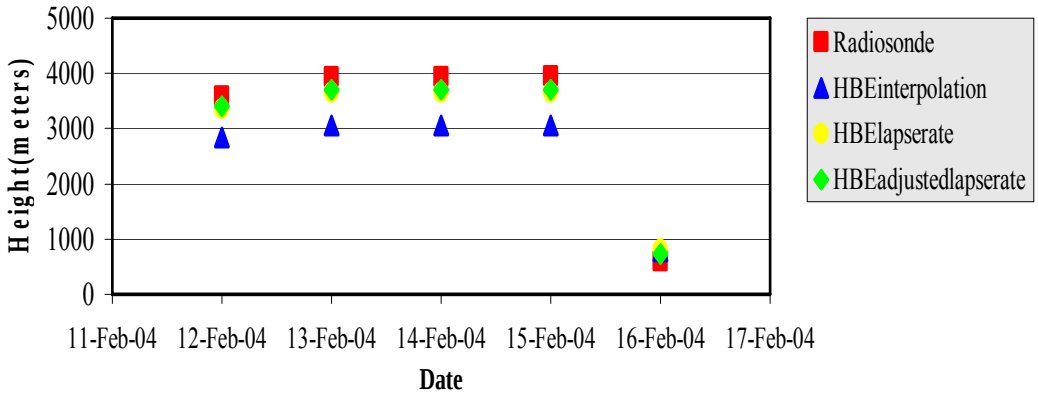

Figure 5.2 Cloud top heights estimated by the different methods.

From the results, lower cloud cover was observed during February 12, 2004. Higher cloud cover was observed during February 14, 2004 and February 15, 2004. Higher precipitation activity was observed during February 14, 2004. Clouds associated with precipitation activity measured about 3500 meters. Estimated cloud top heights indicate the presence of low clouds over the San Juan area at a resolution of 1km. Higher difference between radiosonde observations and the Hydrostatic Balance Equation with the lapse rate estimations is less than 300 meters. Higher difference between radiosonde observations and the Hydrostatic Balance Equation with interpolation estimations is about 900 meters. Comparing both differences, there is about 600 meters difference between the derivations of the hydrostatic balance equation.

The next step to validate MISR and MODIS cloud top heights was the cross-comparison of stereo heights and converted MODIS cloud top pressures into heights. The sample images in Figure 5.3 correspond to December 24, 2000 during 15:10 – 15:15 UTC: calculated cloud top heights from MODIS and Stereo Heights SDS (Blocks 62-80) latitude 13.1 N, 35.6 S, longitude -66.2 W, -60.6 E from MISR

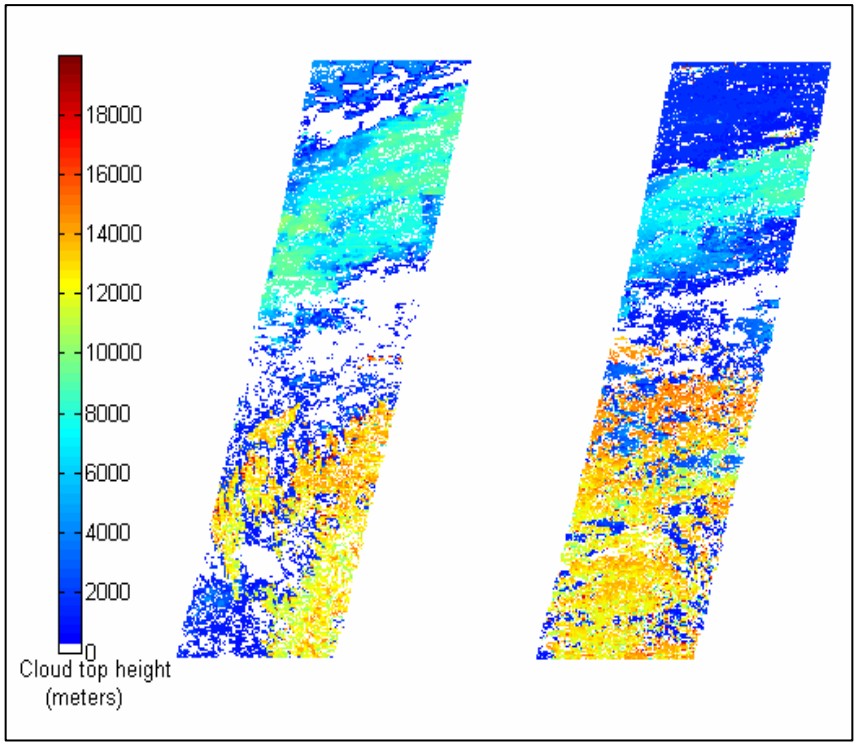

Figure 5.3 MODIS cloud top heights and MISR stereo heights.

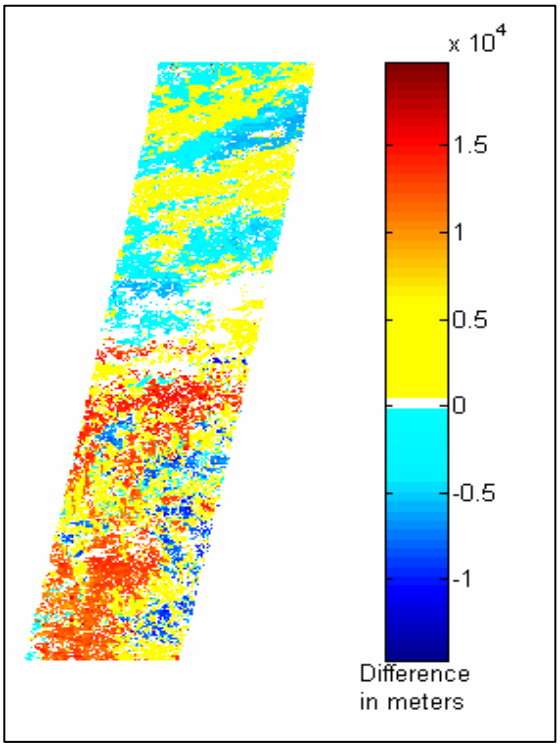

Figure 5.4 Cross-comparison between MODIS cloud top heights and MISR stereo heights.

MISR cloud top heights can be approximately 2 to 4 kilometers higher than MODIS cloud top heights. Other variations between MODIS and MISR cloud top heights may indicate the retrieval of two different cloud heights over the same area. Highest error between MISR and MODIS high clouds vary between 15 and 19 kilometers (see Figure 5.5). This observation may indicate that one of the instruments was detecting a low cloud. Over 9000 meters, MODIS detects higher cloud tops than MISR in 13.98% of the total observed area. But MISR detects higher cloud tops than MODIS in 26.89% of the total observed area. MISR retrieval performance for high clouds is twice the MODIS retrieval performance. MISR and MODIS cloud values coincide in less than 1% of the total observed area and the cloud height value is 14km.

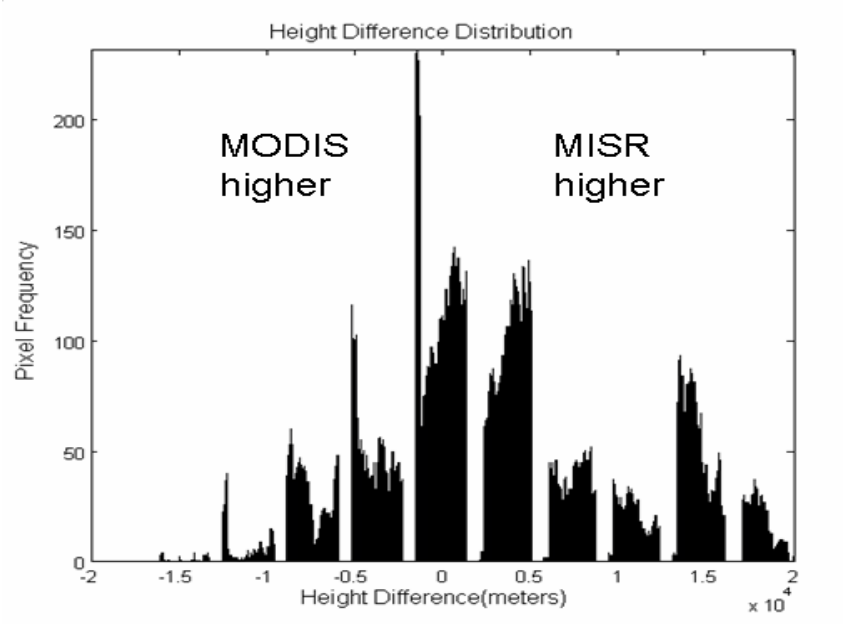

Figure 5.5 Histogram of cloud top height difference pixel distribution.

6 CONCLUSIONS

The difference between MODIS and MISR cloud top heights can be as highest as 2 to 4 kilometers. Because MODIS CO_2 slicing algorithm is applied to clouds at pressures lower than 700 hPa, low-level cloud heights are based under the assumption that the cloud is optically thick. Multi-layered clouds can't be detected in MODIS because the algorithm also assumes a single cloud layer in the field of view. In consequence, thin cirrus clouds will not be identified due to their lower water content.

MISR stereo height algorithm detects better high clouds. The ability to view at different angles enables the MISR sensor to detect high thin cirrus clouds. MISR will have a better retrieval performance because it will be able to detect thin clouds when multilayer clouds appear and it will detect higher clouds than MODIS. Overall results from MISR for the detection of high clouds coincide with [Naud et al., 2004]. The author also found that optically thin clouds were found to be accurately characterized by the MISR cloud top height product by making comparisons over the British Isles.

7 FUTURE WORK

Future work will be the use of lidar instrumentation to validate MODIS cloud top heights. It should be expected to validate MODIS mid and low cloud top heights over a geographic location in Puerto Rico by using available lidar observations from the same time constraints the MODIS instrument overpasses Puerto Rico. Also cross-comparisons with MODIS, MISR and ICESat (Ice, Cloud and Land elevation Satellite) will be done. ICESat data provide cloud altitude and cloud thickness. In the near future, comparisons will be made with preliminary results of the mission CALIPSO (Cloud-Aerosol Lidar and Infrared Pathfinder Satellite Observation).

BIBLIOGRAPHY

Baum, Bryan A., R. A. Frey, S. Ackerman, and W. P. Menzel, 2002. *Remote Sensing of Global Cloud Properties Using MODIS Data*. IEEE International Geoscience and Remote Sensing Symposium, vol. 2: 1183-1184.

Berendes, T.A., D.A Berendes, R.M. Welch, E.G Dutton, T. Uttal, and E.E Clothiaux, 2004. *Cloud cover comparisons of the MODIS daytime cloud mask with surface instruments at the north slope of Alaska ARM site.* IEEE Transactions on Geoscience and Remote Sensing, 42(11): 2584 – 2593.

Bothwell, G. W., Earl G. Hansen, Robert E. Vargo, and Kyle C. Miller, 2002. *The Multi-Angle Imaging Spectroradiometer science data system, its products, tools, and performance*. IEEE Transactions on Geoscience and Remote Sensing, 40(7):1467-1476.

Davis, J.C., J.X. Tull, J.J. Lisowski, and T. Caldwall, 2000. *Cloud characterization in the S/MWIR using a linear least squares algorithm.* IEEE Proceedings from the Aerospace Conference, 18-25 March 2000, vol.3: 351 – 364.

Devasthale, A., O. Kruger, and H. Grassl, 2005. *Change in cloud-top temperatures over Europe.* IEEE Geoscience and Remote Sensing Letters, 2(3): 333-336.

Gang Hong, G. Heygster, and K. Kunzi, 2005. *Intercomparison of deep convective cloud fractions from passive infrared and microwave radiance measurements.* IEEE Geoscience and Remote Sensing Letters, 2(1): 18-22.

Gao, Bo-Cai, Ping Yang; Guang Guo, S.K. Park, W.J. Wiscombe, and Baode Chen, 2003. *Measurements of water vapor and high clouds over the Tibetan Plateau with the Terra MODIS instrument*. IEEE Transactions on Geoscience and Remote Sensing, 41(4): 895 – 900.

Gao, Bo-Cai, Ping Yang, Wei Han, Rong-Rong Li, and Warren J. Wiscombe, 2002. *An Algorithm Using Visible and 1.38μm Channels to Retrieve Cirrus Clouds Reflectances From Aircraft and Satellite Data*. IEEE Transactions on Geoscience and Remote Sensing. 40(5):1-10.

González, J. E., J.C. Luvall, D. Rickman, D. Comarazamy, A.J. Picón, E.W. Harmsen, H. Parsiani, N. Ramírez, R. E. Vásquez, R. Williams, R. B. Waide, and C.A. Tepley. *Urban Heat Islands Developing in Coastal Tropical Cities.* Eos Weekly Newspaper, American Geophysical Union, Vol. 86, Num. 42, October 15, 2005.

Griffin, M., H. Burke, D. Mandl, and J. Miller, 2003. *Cloud cover detection algorithm for EO-1 Hyperion imagery.* IEEE Proceedings from the International Geoscience and Remote Sensing Symposium, IGARSS'03, vol.1: 86-89.

Hawkinson, James A., Wayne Feltz, Timothy J. Schmit, Anthony J. Schreiner and Steven A. Ackerman, 2003. *A Validation Study of the GOES Sounder Cloud Top Pressure Product*, American Meteorological Society Annual Meeting, P. 3.37.

Horváth, Ákos and Roger Davies, 2001. *Simultaneous retrieval of cloud motion and height from polar-orbiter multiangle measurements*, Geophysical Research Letters, 28(15):2915-2918.

Lawton, R.O., U.S. Nair, R.A. Pielke Sr., and R. M. Welch, 2001. *Climatic Impact of Tropical Lowland Deforestation on Nearby Montane Cloud Forests.* Science Magazine, vol. 294: 584-587.

Loyola, D., 2001. *Inverse modeling with neural networks for the retrieval of cloud parameters*. IEEE Proceedings from the International Geoscience and Remote Sensing Symposium, IGARSS'01, vol. 3: 1155 – 1157.

Loyola, D.G.R., 2004. *Automatic cloud analysis from polar-orbiting satellites using neural network and data fusion techniques.* IEEE Proceedings from the International Geoscience and Remote Sensing Symposium, IGARSS'04, vol. 4: 2530 – 2533.

Menzel, P. and K. Strabala. *Cloud-top properties and cloud phase algorithm theoretical basis document*, October 1997, version 5.

Moroney, Catherine, Roger Davies, and Jan-Peter Muller, 2002. *Operational Retrieval of cloud-top heights using MISR data*. IEEE Transactions on Geoscience and Remote Sensing, 40(7):1532-1540.

Muller, J.-P., A. Mandanayake, C. Moroney, R. Davies, D. J. Diner, and S. Paradise, 2002. *MISR stereoscopic image matchers: Techniques and results*, IEEE Transactions Geoscience and Remote Sensing, 40(7): 1547–1559.

Nair, U.S., R.M. Welch, R.O. Lawton, and R.A. Pielke Sr., 2000. *Impact of land use on Costa Rican regional climate.* IEEE Proceedings from the International Geoscience and Remote Sensing Symposium, IGARSS'00, vol. 5: 1993 – 1995.

Naud, C., J.P. Muller and E.E. Clothiaux, 2002. *Comparison of cloud top heights derived from MISR stereo and MODIS CO_2 slicing*. Journal of Geophysical Research Letters, vol. 29, no. 16, 42:1-4.

Naud, C., J.P. Muller, M. Haeffelin, Y. Morille and A. Delaval, 2004. *Inter-comparison of MERIS, MODIS and MISR cloud top heights*. Journal of Geophysical Research Letters, vol. 31, L04114.

Nieman, Steven J., Johannes Schmetz and W. Paul Menzel, 1993. *A Comparison of Several Techniques to Assign Heights to Cloud Tracers*, Journal of Applied Meteorology, 32(9), pp.1559-1568.

Platnick, Steven, Michael D. King, Steven Ackerman, W. Paul Menzel, et al., 2003. *The MODIS Cloud Products: Algorithms and Examples From Terra*, IEEE Transactions on Geoscience and Remote Sensing, 41(2): pp. 459-473.

Picón, A.J. and R. Vasquez, 2003. *A study on cloud-top height retrieval by using MISR and MODIS data.* IEEE Proceedings from the International Geoscience and Remote Sensing Symposium, IGARSS'04, vol. 2: 872 – 874.

Picón, A. J. and R. Vásquez, 2004. *Retrieval of cloud-top heights over the Caribbean*. Proceedings of Remote Sensing of Clouds and the Atmosphere IX Conference, vol. 5571: 424-432.

Schutz, B. E., 2001. *Laser Altimetry and Lidar from ICESat/GLAS*. IEEE International Geoscience and Remote Sensing Symposium, vol. 3:1016-1019.

Tao Shi, Bin Yu, E. Clothiaux, and A. Braverman, 2004. *Fusing information from MISR and MODIS for polar cloud detection.* Conference Record of the Thirty-Eighth Asilomar Conference on Signals, Systems and Computers, vol. 2: 1705 – 1709.

Tian, B., M. R. Azimi-Sadjadi, T.H. Vonder Haar and D. Reinke, 1997. *Neural Network-Based Cloud Classification on Satellite Imagery Using Textural Features.* IEEE Transactions on Geoscience and Remote Sensing, pp.209-212.

Vanbauce, C., R. Cadet, and R. T. Marchand, "Comparison of Polder apparent and corrected oxygen pressure to ARM/MMCR cloud boundary pressure", *Journal of Geophysical Research Letters*, vol. 30, no. 5, 2003, 16:1-4.

Wang, James R., Paul Racette, M. E. Triesky, and Will Manning, 2002. *Retrievals of Column Water-Vapor Using Millimeter-Wave Radiometric Measurements*. IEEE Transactions on Geoscience and Remote Sensing, 40(6): 1220-1229.

Wilson, M.J., and L. Di Girolamo, 2004. *The utilization of MISR for polar cloud modeling*. IEEE Proceedings from the International Geoscience and Remote Sensing Symposium, IGARSS'04, vol. 7: 4361 – 4362.

Xiaoning Song, Zhenhua Liu, and Yingshi Zhao, 2004. *Cloud detection and analysis of MODIS image.* IEEE Proceedings from the International Geoscience and Remote Sensing Symposium, IGARSS'04, vol. 4: 2764 – 2767.

Yasumoto, M., S. Mukai, and I. Sano, 2001. *Cloud properties retrieved from ADEOS/POLDER and OCTS*. IEEE Proceedings from the International Geoscience and Remote Sensing Symposium, IGARSS'01, vol. 3: 1052 – 1054.

Zong, Jia, Roger Davies, Jan-Peter Muller, and Davis J. Diner, 2002. *Photogrammetric retrieval of cloud advection and top height from the Multi - Angle Imaging Spectroradiometer (MISR),* Photogrammetric Engineering & Remote Sensing, 68(8):821-829.

APPENDIX A. MISR DATA VISUALIZATION AND MANAGEMENT

Because of the complexity of the hierarchical data formats (hdf), some specialized software tools must be used to read and manage satellite sensors data. MISR data can be managed with an IDL program called MISR_VIEW. This program was designed by the NASA Jet Propulsion Laboratory (JPL) for use with those MISR and AirMISR files that use the HDF-EOS "grid" interface. These files include MISR L1B2 georectified (map-projected) radiances, MISR L1B3 radiometric cloud masks, all MISR Level 2 products, the MISR Ancillary Geographic Product, and AirMISR L1B2 georectified radiances. In the case of MISR data visualization, the user interface provides data selection for specified orbits, paths, or observation dates, and enables translation between these modes of identification. In the case of AirMISR data, the user interface is simplified. The display and analysis tools include simultaneous display of several data planes through color assignment, contrast enhancement, pseudo coloring, data value query, image rotation, creation of stereo anaglyphs, zooming, linked analysis and view windows, vector overlays and map projections. The interface supports simultaneous viewing of three data planes in color where the different planes may have different native number types and different spatial resolutions. Additionally, there are three ancillary planes which can be populated with data for analysis, and any of these planes may be reassigned to any of the three color planes. Eight bit displays are supported through 24-bit emulation. Data with different number types and disparate spatial resolutions in each of the data planes will be displayed correctly. It also supports data transforms that are

useful for scaling and unpacking MISR data. Data is stored internally as its native number type and native spatial resolution for accurate analysis and memory efficiency.

A.1 Reading MISR data in MISR_VIEW software tool

The user interface provides the selection, displaying and analyzing of MISR gridded datasets. The user can select any available orbits, paths, blocks, and parameters through the use of its data selection interface. Once grid data is displayed, it can be zoomed in or out, panned, linked to other grid data displays, have the DN values scaled, have vectors overlaid and be map projected.

To starting up the program, it must be invoked from an IDL command window. The misr_view software pack includes a README file with the specifications to run the program in the IDL environment. When the misr_view interface appears, it looks like Figure A.1. To open a data file, the user must go to the main console and click on **Controls->Open MISR Catalog/File** (see Figure A.2). Then select either a MISR HDF-EOS grid file or an existing misr_view catalog file. The program will automatically identify if the source is MISR or AirMISR, the orbit date, the path and the orbit GMT hour. It will also recognize the geographic area covered by the path. By selecting the **Choose MISR Blocks** toggle button, the desired starting and ending block values in the **Start Block** and **End Block** text entries can be specified, respectively. Then with the *Enter* key the new block values are registered and the map is updated, which may be used interactively to select blocks by dragging the lines north and south.

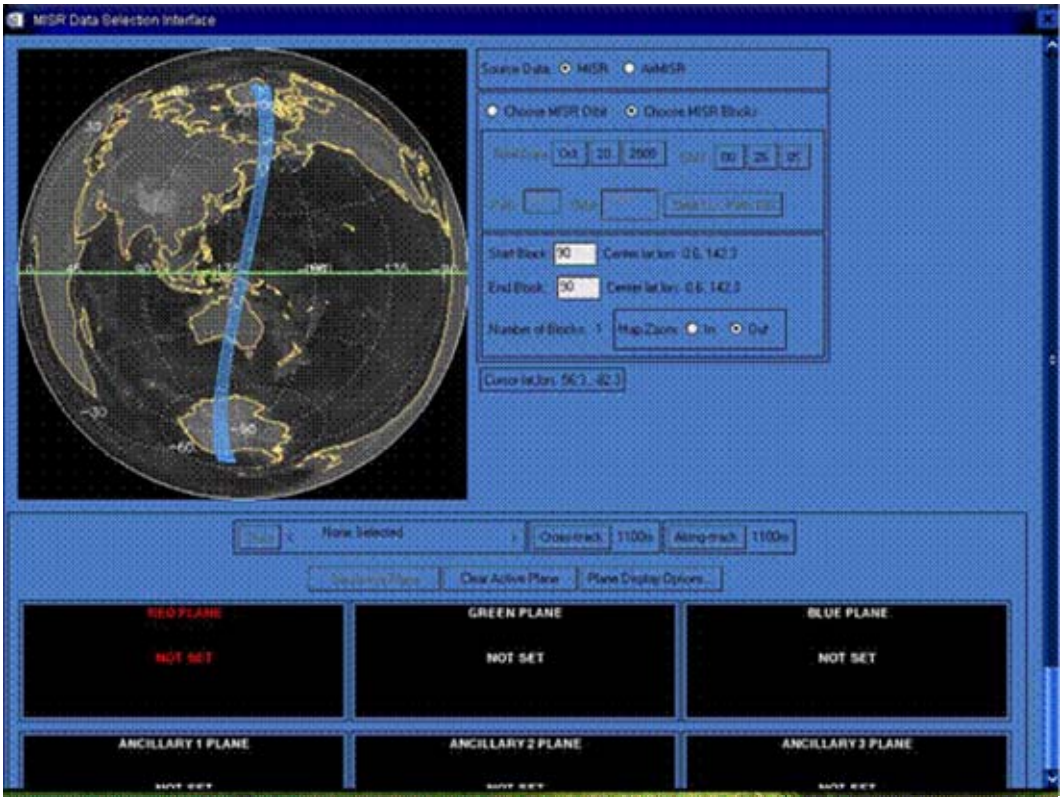

Figure A.1 MISR_VIEW user interface.

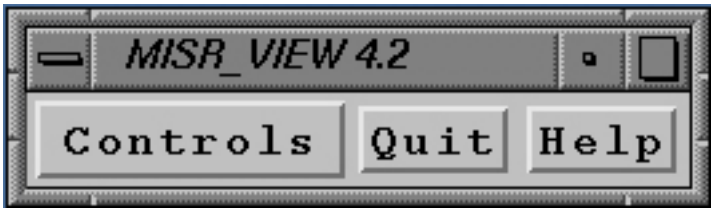

Figure A.2 MISR_VIEW main console.

To select parameters, on the data selection interface, click on the **Data** button; then, in the MISR Data Menu interface(Figure A.3), click on the desired product, grid, and field to be displayed from the respective lists (also click on the desired dimensions if the selected field has dimensions other than XDim, YDim, and SOMBlockDim). Click on **OK** to dismiss the MISR Data Menu interface. A concatenated text string representing

the currently-selected product, grid, and field will be displayed in the data selection interface adjacent to the **Data** button.

Figure A.3 MISR data parameters selection window.

Every MISR data parameter has six associated "data planes". The user can assign parameters to one or all of the planes, but only three planes maximum can be viewed simultaneously. To load the current parameter into one of these planes, click on one of the six plane widgets located in the bottom half of the data selection interface(see Figure A.4); the text within the plane widget should turn red, green, blue or lavender, depending on which plane was selected. Click on the **Set Active Plane** button to assign the current parameter to the active data plane (the text within the active plane widget should update

to reflect its contents). The spatial resolution of the data can be updated by clicking on the **Cross-track** and **Along-track** toggle buttons. The plane widgets should automatically update their text to reflect any changes made using the resolution buttons.

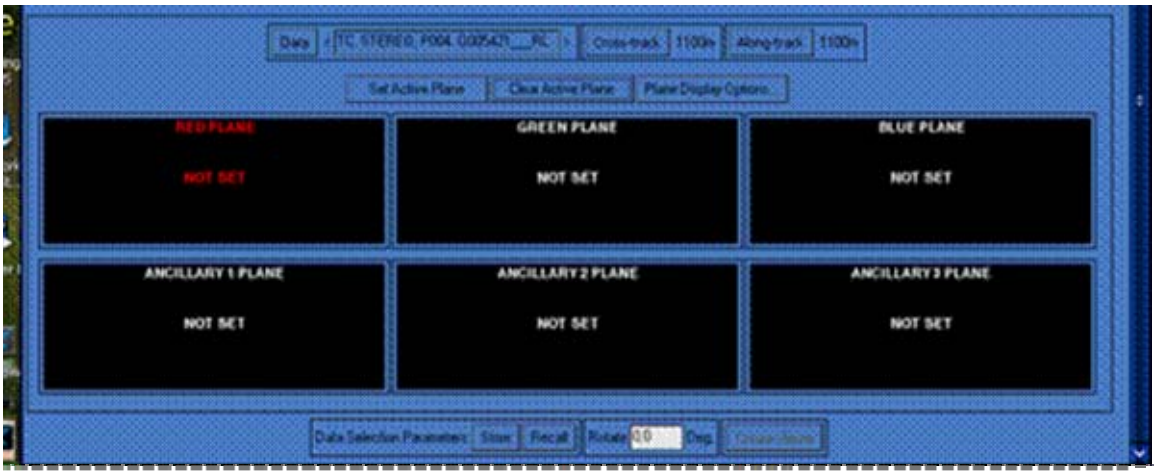

Figure A.4 Viewing planes that can be associated with a data parameter.

After all orbit, path, block, and parameter information has been specified, click on the **Create Viewer** button located at the bottom of the data selection interface. The selected parameter will be viewed in a new data window (see Figure A.5). The data displayer is interactive and the user can manipulate their contents via several modes and utilities which are available through the data window menu, toggled on and off by clicking the right-hand mouse button within the data window display area. The standard data window's menu bar contains the following four menus: **Utilities**, **Tools**, **Modes**, and **Kill**. Every data window will have a companion window which displays and continually updates the longitude, latitude, block number, block-x, block-y, and data values at the location of the cursor whenever it is within the data display region of the window. By clicking on the **Utilities→Save Data,** the displayed data information can be saved as an

scientific data set in .hdf format. This new dataset can be easily opened in ENVI or Matlab software.

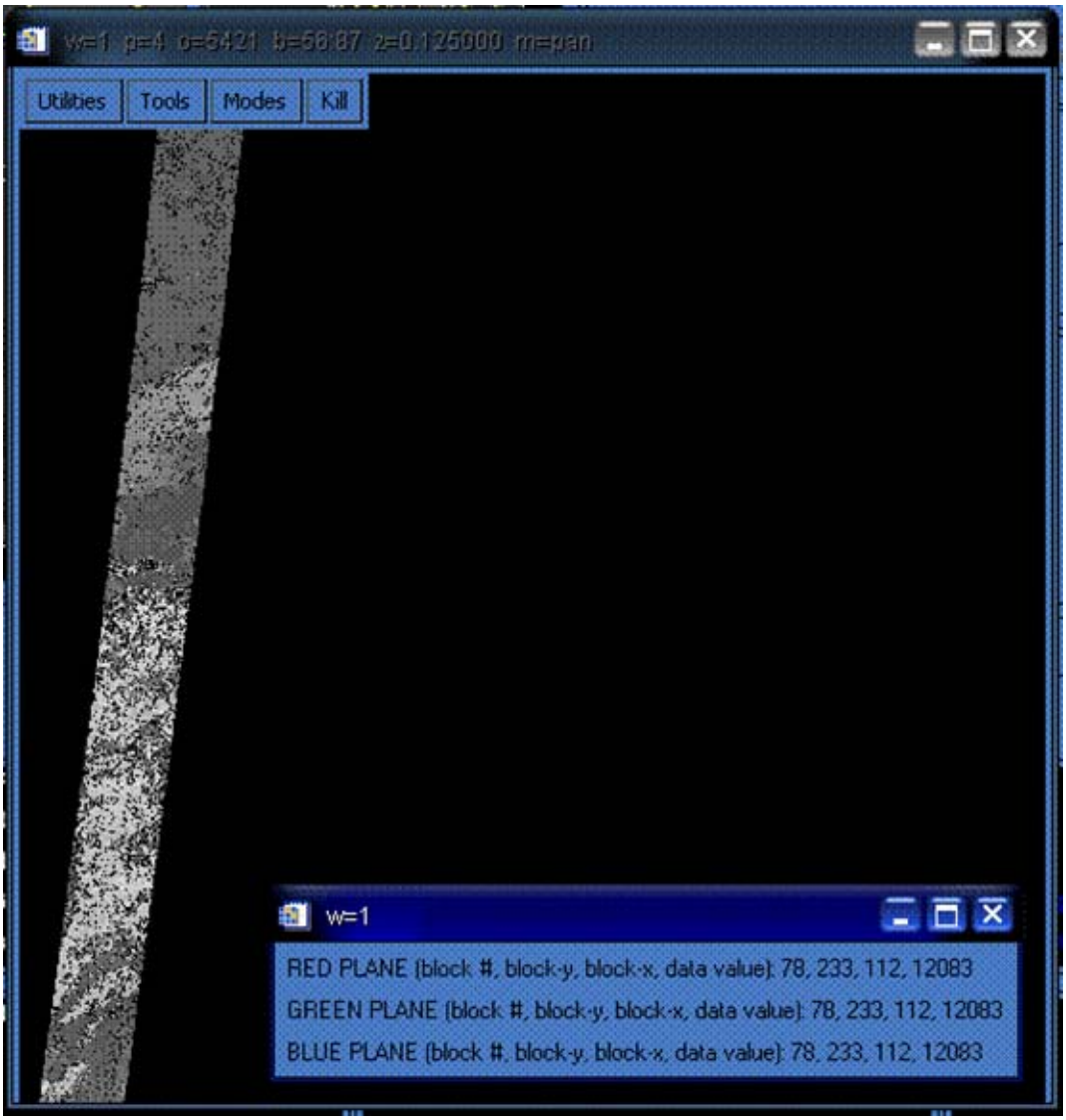

Figure A.5 Data window and companion window (lower right).

There are some tools that can be used to visualize the data information such as the perspective viewing, the band slider tool, the scroll tool and the vector overlay tool. The data window can be zoomed also. To dismiss the data window, **Kill** must be clicked.

A.2 Reading MISR data in ENVI and Matlab

Basically the extraction of the specified data can be performed by MISR_VIEW. Then the new file saved as an .hdf extension can be open by ENVI and Matlab. ENVI means the Environment for Visualizing Images. It is an image processing system. It was designed in response to the numerous and specific needs of satellite and aircraft remote sensing data users. It provides comprehensive data visualization and analysis for images of any size and any type.

When open an .hdf extension of MISR in ENVI, first click on the **File** menu and then click **Open Image File.** After selecting the file to be opened, a window called HDF Dataset Selection will appear (see Figure A.6). The user should indicate the dataset that was previously saved in the MISR_VIEW module. When a file is opened for the first time during a session, ENVI automatically places the filename, with all of its bands listed beneath it, into the Available Bands List (see Figure A.7).

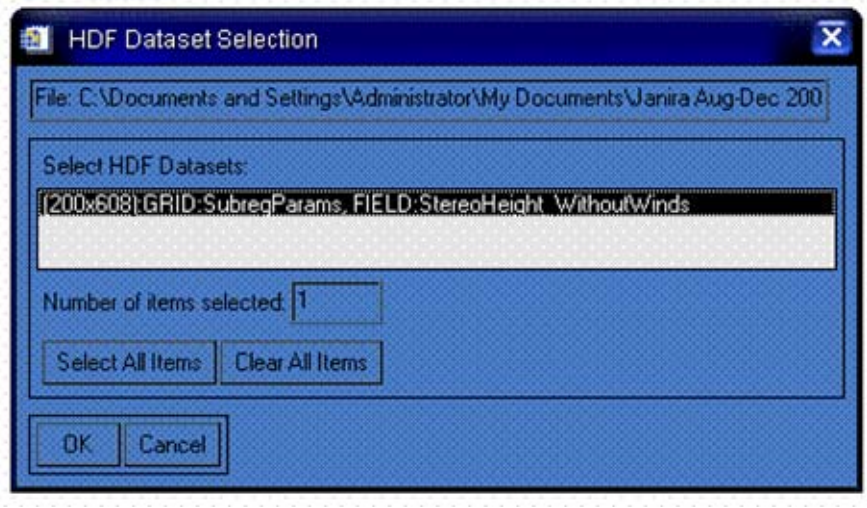

Figure A.6 HDF dataset selection window.

Figure A.7 Available bands list window.

When no display window is open, the button at the bottom of the Available Bands List reads No Display. The first image loaded automatically appears in a new window. To display the image, just click **Load Band** label to load the selected band which in this case is the MISR saved dataset. The loaded image will have three different windows: the main image, the scroll and the zoom (see Figure A.8). The Main Image window displays a portion of the loaded image at full resolution. Dynamically the Main Image window can be resized up to the available screen size by grabbing one of the corners and dragging to the desired image size. The Scroll window is a small image display window that appears

when the display window style is set to Scroll/Zoom or Scroll/Image/Zoom and the main image is larger than can be displayed in the Main Image window at full resolution. The image in the Scroll window is displayed at subsampled resolution. The resampling factor appears in parenthesis in the title bar. The Main Image window indicator appears as a box within the scroll window and outlines the area that is displayed in full resolution in the Main Image window. The Zoom window is a small image display window that displays a portion of the image at a user-defined zoom factor.

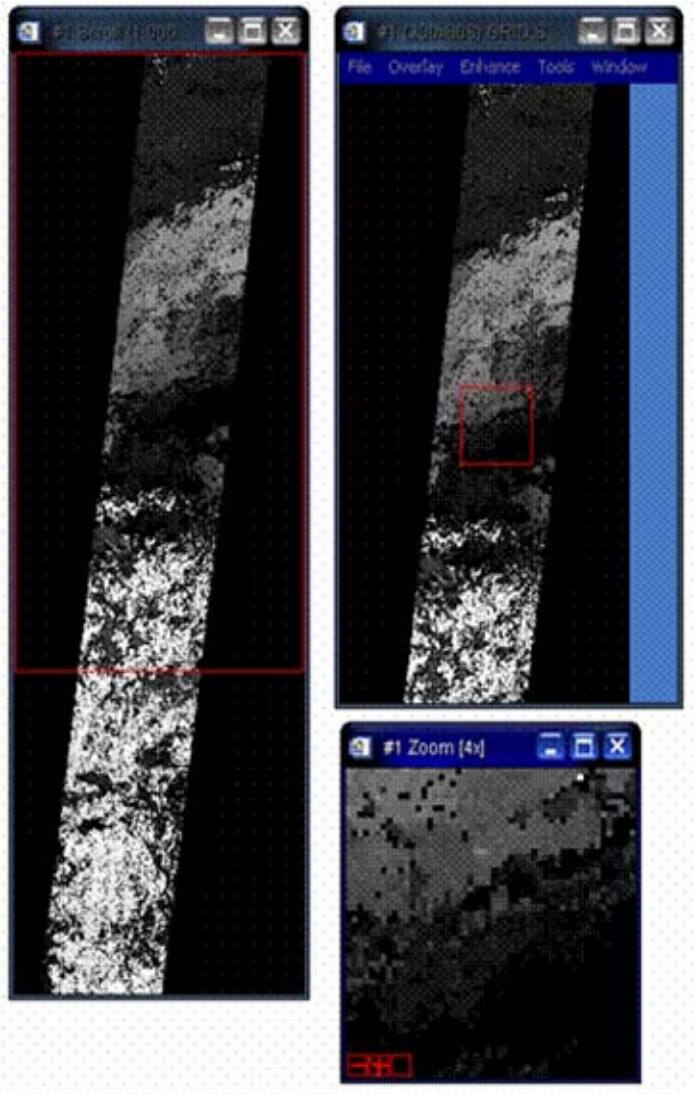

Figure A.8 Main image, scroll and zoom windows.

By using **Save File As,** a new file can be created to output image data to various image processing formats such as ArcView Raster (.bil), PCI (.pix), ER Mapper, NITF (.ntf), and ERDAS (.lan) and TIFF files (including GeoTIFF and TIFF world files [.tfw]). Also the image can be outputted as an ASCII (.txt) file.

Matlab offers a different image processing environment which is more technical computing oriented. In Matlab, the MISR saved dataset will open in a HDF import tool(see Figure A.9). By clicking on the Import button, the selected dataset will be imported to the workspace window. The imported dataset will appear as an integer matrix in the workspace window(see Figure A.10). Having the imported dataset in the workspace window will facilitate its use in the different subroutines written in Matlab. The datatype of the imported dataset must be changed to manipulate the data.

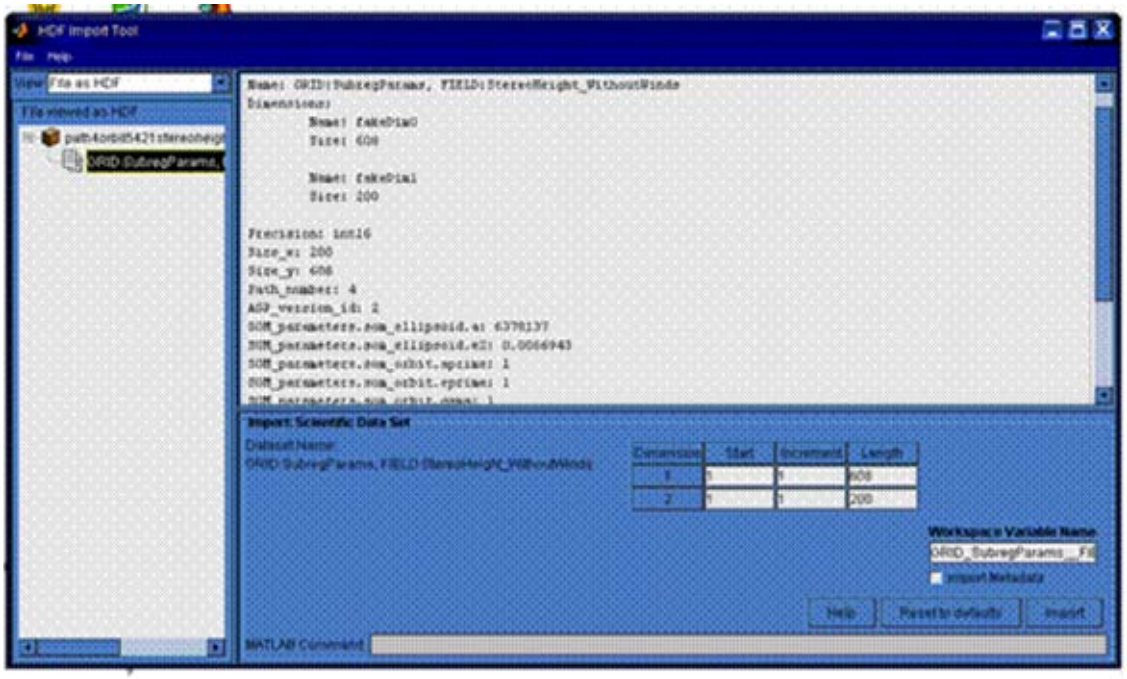

Figure A.9 Matlab HDF import tool window.

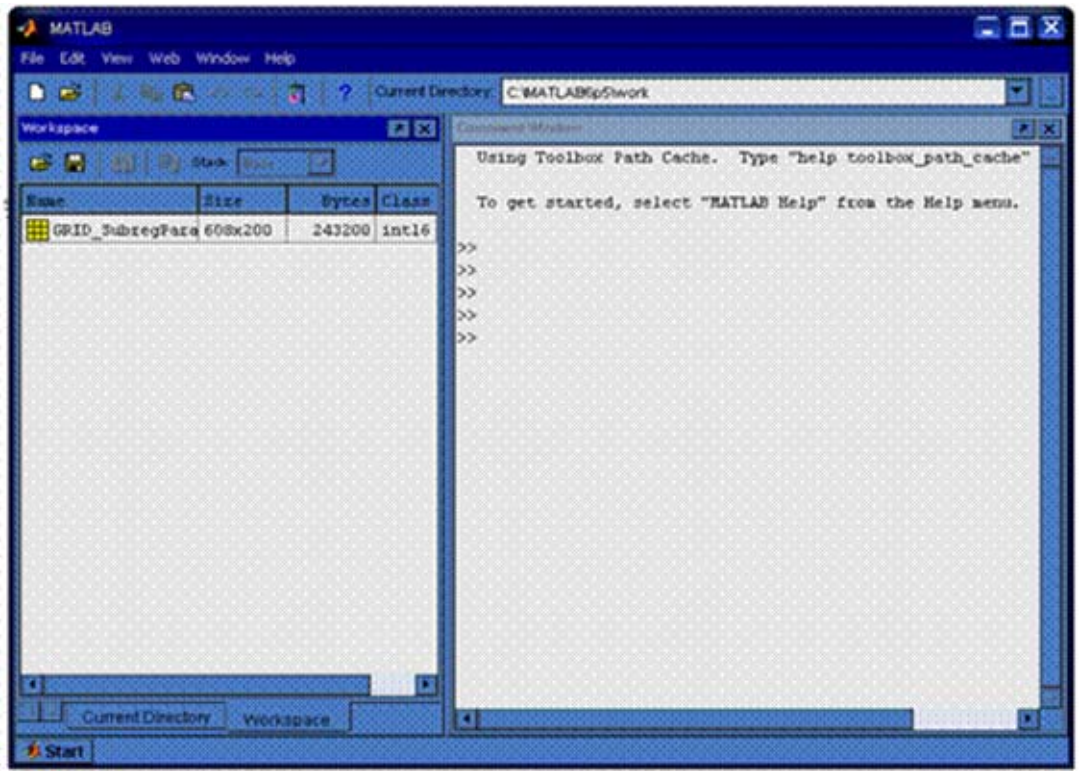

Figure A.10 Matlab main console that shows the command, the current directory and the workspace windows.

APPENDIX B. MODIS DATA VISUALIZATION AND MANAGEMENT

MODIS operational cloud product is a different hierarchical data format (hdf) that can be opened by ENVI and Matlab software tools. MODIS products come with latitude and longitude information. In the case of the MISR products, the tool MISR_VIEW automatically opened the corresponding dataset georeferenced. MODIS datasets need to be georeferenced. Because MISR spatial resolution can be resized up to 4.4 kilometers and MODIS cloud product is 5 kilometers, resizing is another operation that needs to be performed. With the use of ENVI, MODIS cloud properties datasets can be georeferenced, resized and saved to be open by Matlab and other image software.

B.1 Reading MODIS data in ENVI software tool

To open a MODIS data product, the user needs to open an image file by clicking the **File** menu and **Open Image File.** After selecting the file to be opened, a window called HDF Dataset Selection will appear (see Figure B.1). The user should indicate the datasets that needs to be opened such as the Geodetic Latitude, the Geodetic Longitude and Cloud Top Pressure. When a file is opened for the first time during a session, ENVI automatically places the filename, with all of its bands listed beneath it, into the Available Bands List (see Figure B.2). When no display window is open, the button at the bottom of the Available Bands List reads No Display. The first image loaded automatically appears in a new window. To display the image, just click **Load Band**

label to load the selected band which in this case is the MODIS dataset. The loaded image will have three different windows: the main image, the scroll and the zoom.

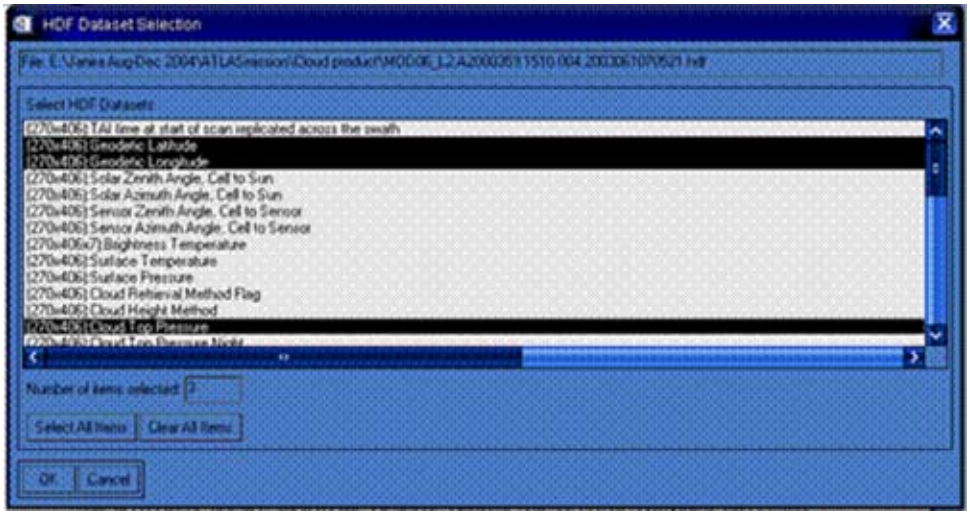

Figure B.1 HDF dataset selection window to select MODIS data parameters.

Figure B.2 Available bands list window after opening MODIS datasets.

B.2 Georeferencing MODIS data in ENVI software tool

Georeferenciation or registration is the process in which images can be referenced to geographic coordinates and/or corrected to match base image geometry. Because MODIS data products include georeference data that has an associated file containing map locations for every pixel, one of the map registration tools that provides ENVI can be used to registrate a specified dataset. This is a very accurate method of georeferencing data because it places every pixel at its exact map location. Generally the map information is stored in two bands, one for X coordinates (e.g., longitude or northing) and one for Y coordinates (e.g., latitude or easting). The file that contains this information is called the input geometry (IGM) file. Remember MODIS products include geodetic latitude and geodetic longitude information, so the IGM file will be the product file that includes the X and Y coordinates.

As mentioned before the IGM is not geocorrected, but does contain the geolocation information for each original raw pixel. ENVI uses the IGM file to create a geographic look-up table (GLT) file that contains the information about the correspondence of every original pixel with the output pixel in the final product. The GLT file can be used to geocorrect any band or derived product through a lookup table. The GLT file contains a fixed pixel size projected into a rotated UTM system. It uses 1-based coordinates (upper left pixel is located at 1, 1).

The first step to georeference a MODIS cloud properties dataset is building a GLT file. In the **Map** menu, click on **Georeference from Input Geometry** and use **Build GLT** to build the Geographic Lookup Table (GLT) file. When the Input X Geometry

Band selection dialog appears, select the band that contains the X geometry coordinates that is the Geodetic Longitude parameter from the MODIS cloud product and then click OK (see Figure B.3). When the Input Y Geometry Band selection dialog appears, select the band that contains the Y geometry coordinates that is the Geodetic Latitude parameter from the MODIS cloud product and then click OK (see Figure B.4). The Geometry Projection Information dialog appears (see Figure B.5). In the Input Projection of Geometry Bands list, click on the projection type. In the Output Projection for Georeferencing list, click on the projection for the georeferencing. It is very important to maintain consistency in the projection type. MODIS must be projected in the same system MISR is projected.

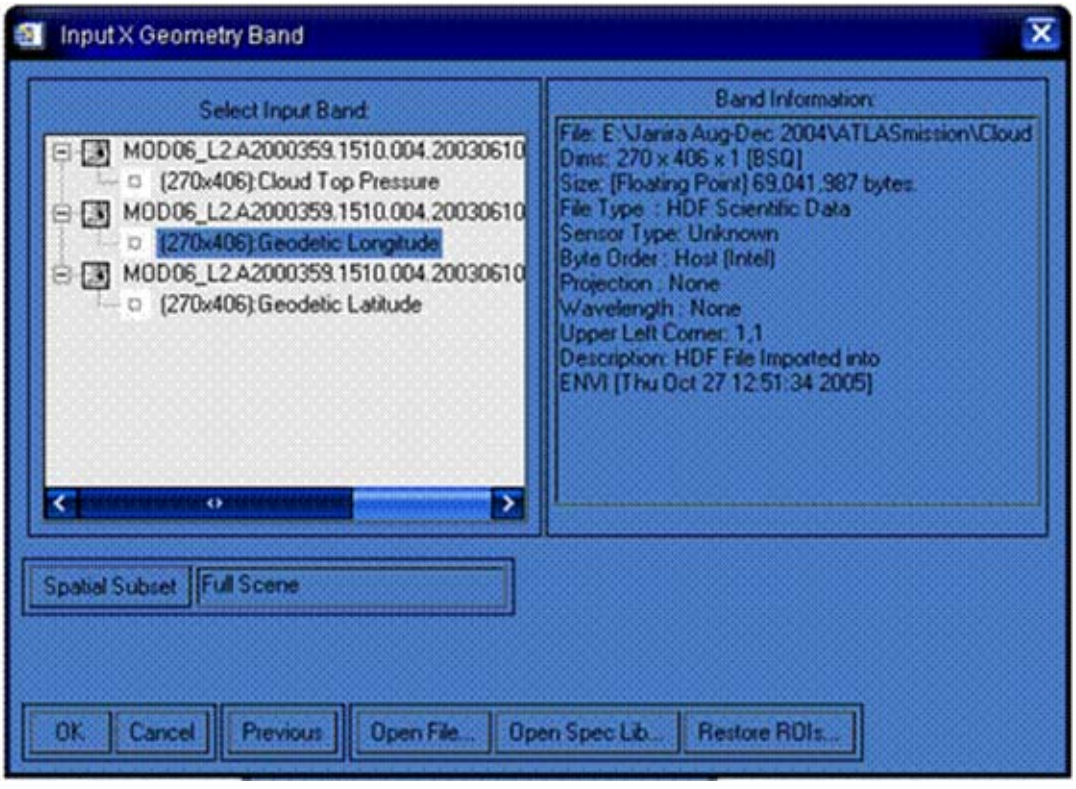

Figure B.3 Input X geometry band selection dialog box.

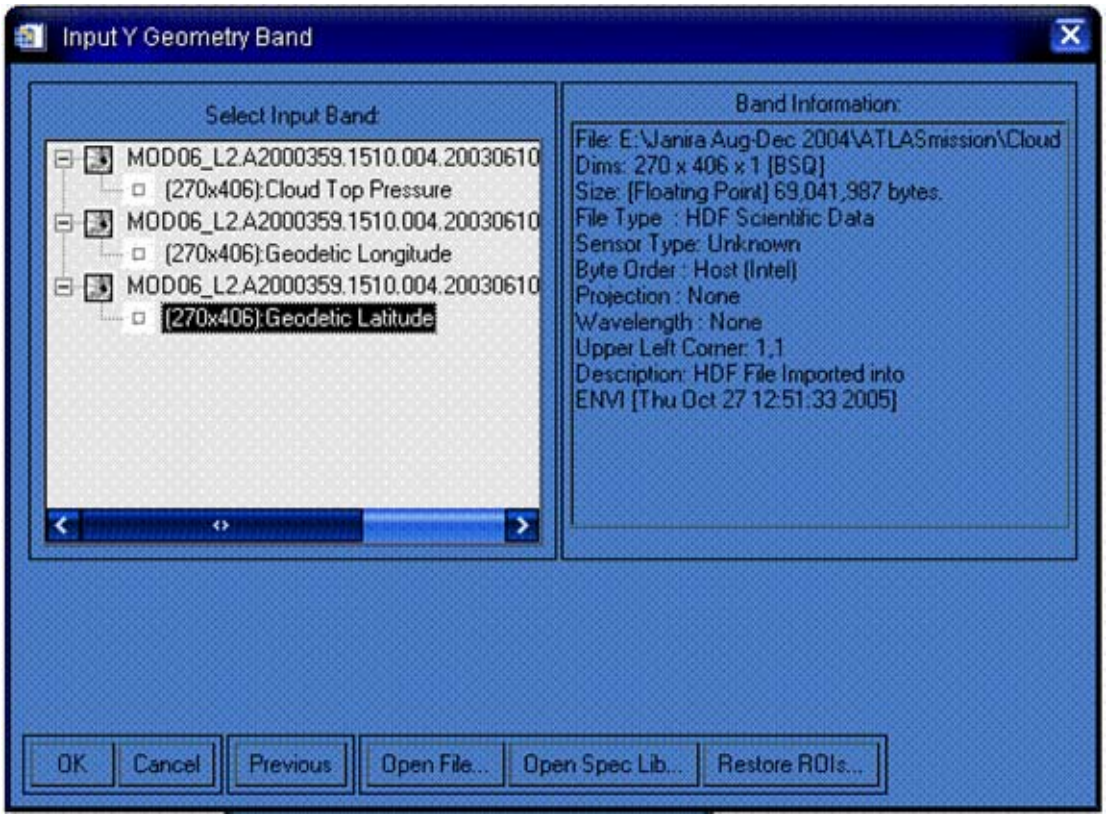

Figure B.4 Input Y geometry band selection dialog box.

After clicking OK, a default output pixel size and rotation angle is calculated and it appears in the Build Geometry Lookup File Parameters dialog (see Figure B.6). The default output pixel size is calculated based on the map coordinates in output space**.** The default output rotation angle is used to minimize the output file size. If the rotation angle is set to 0 then north will be up in the output image. If it is set to another angle, then north will be at an angle and will not be "up" in the output image. The rotation angle is stored in the ENVI header and is used when overlaying grids, so the grid lines will appear at an angle. To change the output pixel size, replace the value in the Output Pixel Size text box. To change the output rotation angle, replace the value in the Output Rotation text box.

Figure B.5 Geometry projection information box.

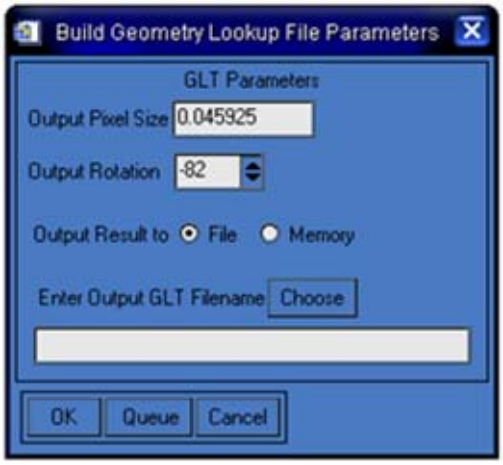

Figure B.6 Build geometry lookup file parameters dialog box.

The process runs in two parts and the output GLT filename appears in the Available Bands List window (see Figure B.7). The two bands of the GLT file refer to the original sample number and the original line number, respectively. The sign of the value indicates whether the pixel is an actual image pixel, located at its proper position (indicated by a positive value) or a nearest-neighbor infill pixel placed to fill an undersampled image gap (indicated by a negative value). A zero value signifies that no input pixel corresponds to the output pixel.

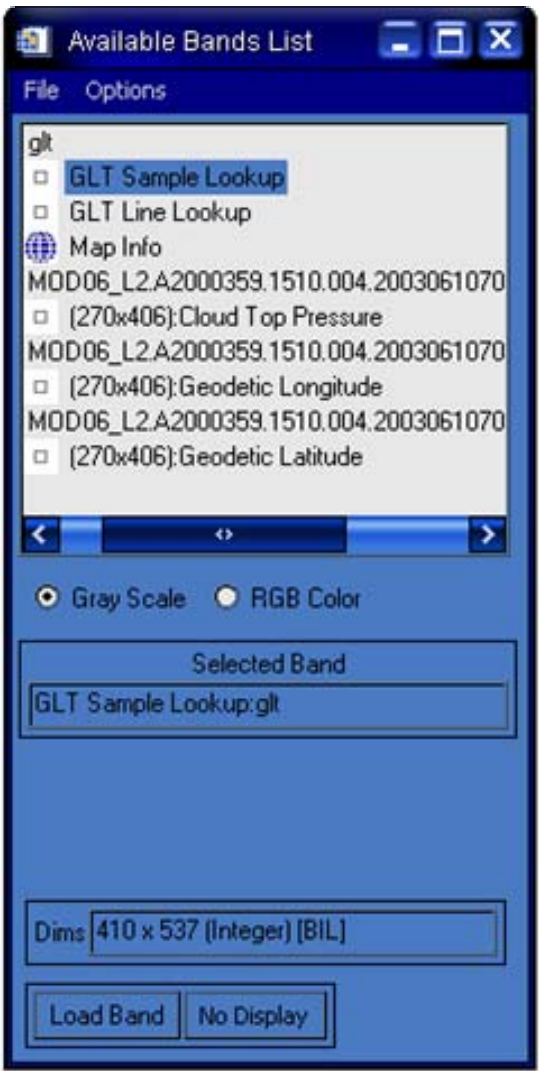

Figure B.7 Available band list window with resulted GLT file.

To finally georeference the image data, go to the **Map** menu, then select Georeference from Input Geometry, and click on Georeference from GLT. Select the GLT file that was previously built. Select the data file to georeference that is the MODIS cloud property dataset. In case the user indicates a subset of the original data as the input file, select whether to output only the warped subset region or whether to output that subset warped within the entire output boundary by clicking the Subset to Output Image Boundary arrow toggle button to select Yes or No. Enter the DN value to use as the background value around the edges of the warped data. Enter an output filename and click OK. The new georeferenced file will appear at the Available Band List window. The file can be loaded for visualization (see Figure B.8).

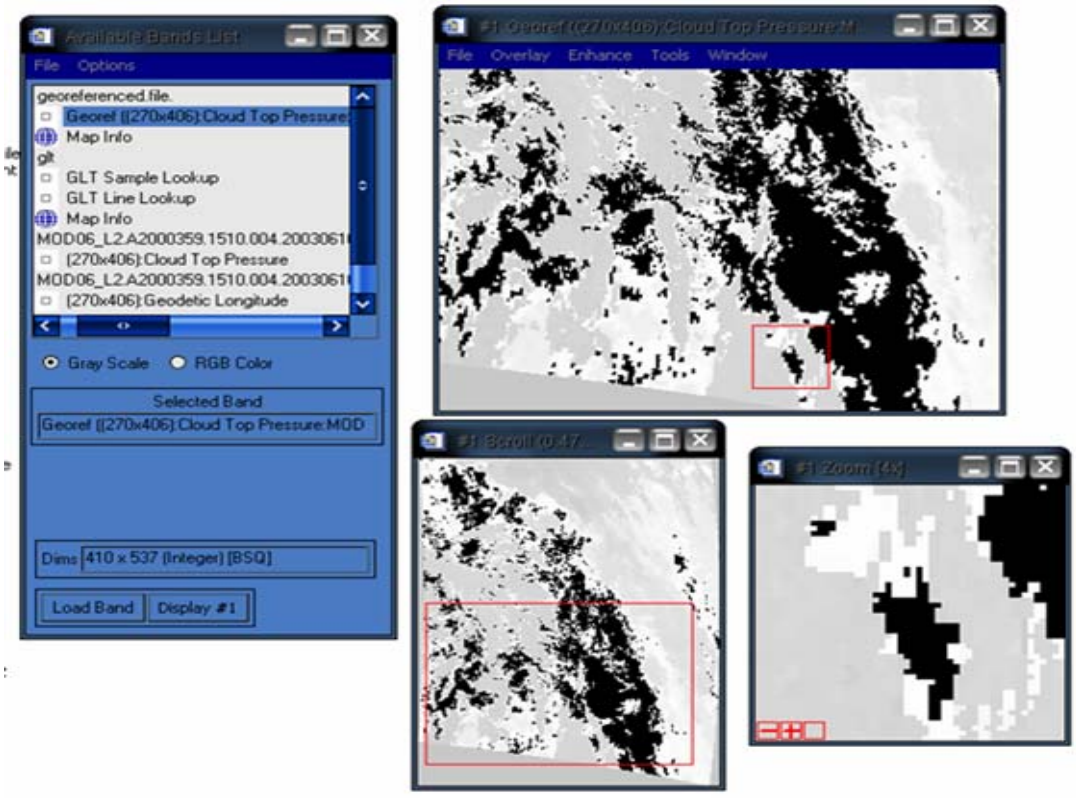

Figure B.8 New georeferenced file in its three view windows: image, scroll and zoom.

B.3 Subsetting MODIS data in ENVI software tool

To extract a specific area of a MODIS image, the data file must be subsetted. ENVI has one tool called layer stacking that can subset and reproject a selected area from the original image. Layer stacking is used to build a new multiband file from georeferenced images of various pixel sizes, extents, and projections. The input bands will be resampled and re-projected to a common user-selected output projection and pixel size. The output file will have a geographic extent that either encompasses the data extent. After subsetting the MODIS image, the file can be converted into a readable Matlab format (see section A.2) such as in the case of MISR.